Multifractal perturbations to multiplicative cascades promote multifractal nonlinearity with asymmetric spectra

Madhur Mangalam [*]
Division of Biomechanics and Research Development, Department of Biomechanics, and Center for Research in Human Movement Variability, University of Nebraska at Omaha, Nebraska 68182, USA

Damian G. Kelty-Stephen [†]
Department of Psychology, State University of New York at New Paltz, New Paltz, New York 12561, USA

(Received 9 February 2024; accepted 24 May 2024; published 17 June 2024; corrected 26 September 2024)

Biological and psychological processes have been conceptualized as emerging from intricate multiplicative interactions among component processes across various spatial and temporal scales. Among the statistical models employed to approximate these intricate nonlinear interactions across scales, one prominent framework is that of cascades. Despite decades of empirical work using multifractal formalisms, several fundamental questions persist concerning the proper interpretations of multifractal evidence of nonlinear cross-scale interactivity. Does multifractal spectrum width depend on multiplicative interactions, constituent noise processes participating in those interactions, or both? We conducted numerical simulations of cascade time series featuring component noise processes characterizing a range of nonlinear temporal correlations: nonlinearly multifractal, linearly multifractal (obtained via the iterative amplitude adjusted wavelet transform of nonlinearly multifractal), phase-randomized linearity (obtained via the iterative amplitude adjustment Fourier transform of nonlinearly multifractal), and phase and amplitude randomized (obtained via shuffling of nonlinearly multifractal). Our findings show that the multiplicative interactions coordinate with the nonlinear temporal correlations of noise components to dictate emergent multifractal properties. Multiplicative cascades with stronger nonlinear temporal correlations make multifractal spectra more asymmetric with wider left sides. However, when considering multifractal spectral differences between the original and surrogate time series, even multiplicative cascades produce multifractality greater than in surrogate time series, even with linearized multifractal noise components. In contrast, additivity among component processes leads to a linear outcome. These findings provide a robust framework for generating multifractal expectations for biological and psychological models in which cascade dynamics flow from one part of an organism to another.

DOI: 10.1103/PhysRevE.109.064212

I. INTRODUCTION

A. Multifractal geometry arising from multiplicative dynamics in biology and psychology

Biology and psychology have begun to explain adaptive behavior as cascades embodying nonlinear interactions across nested spatial and temporal scales [1–3]. Linear modeling of independent effects with normal (Gaussian) patterns of residual variability can be suitable for systems where behaviors result from numerous modular components and exhibit ergodicity, the statistical property of having stable averages. However, measured behaviors in biology and psychology break ergodicity [4–14] and also exhibit nonlinear temporal correlations across multiple spatial and temporal scales entailing non-normal (i.e., non-Gaussian) distributions, such as power laws characterized by scale-invariant tails [15,16]. "Scale invariance" is a mathematical description of how power-law functions have the same form across all intervals of its domain, showing similar or "universal" dynamics across various scales (e.g., seconds, days, and months) and even across different systems, regardless of their material composition [17–19]. Modularity requires appeals to innate, stipulated structure that contemporary biological, evolutionary science make progressively less tenable [20–29]. Power-law patterns offer the alternative that adaptive behavior might arise from relatively generic cascade dynamics enacting nonlinear interactions across scales [30–33]. Nonlinear dynamics propagating across multiple spatial and temporal scales might help to root our understanding of living, behaving systems in the physics of symmetry breaking [34–37] that we might begin to see even through multifractal geometry.

Probing power-law exponents in empirical measurements for evidence of cascadelike nonlinear interactions across scales involves multifractal geometry. Systems exhibiting a single power law are commonly called "fractal" or "monofractal," and cascadelike interactions across multiple scales generate ergodicity-breaking processes with multiple power laws within the same observable, warranting the neologism "multifractal" [38,39]. A classic portrayal of multifractality is the so-called multifractal spectrum, a peaked, often

[*]Contact author: mmangalam@unomaha.edu
[†]Contact author: keltystd@newpaltz.edu

asymmetric, inverted-**U**-shaped curve described by ordered pairs of α and f for each setting of a parameter q; α and f are each power-law exponents describing the change of proportion and Shannon entropy, respectively, with scale [40]. The parameter q allows for the analytical estimation of these power-law exponents for different-sized fluctuations. Positive q, zero-valued q, and negative q estimate these power-law exponents for larger, medium, and smaller fluctuations, respectively, yielding the values for the left, peak, and right sides of the multifractal spectrum. The descriptors from multifractal geometry (e.g., multifractal spectrum width $\Delta\alpha$) provide both an ergodic description that can submit to linear causal models [41–45] and a testable operationalization of how cascades might support adaptive behavior. Multiplicative cascades enact multiplicative relationships across scales by multiplying noise terms defined over coarse and fine scales, and additive cascades enact the same relationship between coarse and fine but with the addition of noise terms, thus leading to none of the nonlinearity observed in multiplicative cascades. The standard statistical test for multiplicative cascadelike nonlinearity assesses $\Delta\alpha$ for the original time series and a sample of surrogate time series, preserving only the time series' linear structure. The difference between the original and surrogate $\Delta\alpha$ is multifractal evidence of cascadelike nonlinear interactions across scales.

The multifractal evidence of cascadelike nonlinear interactions across scales has consistently foreshadowed adaptive behaviors in various domains: postural control [46–49], brain function [50,51], cognition [52–54], and perceptuomotor responses [55–64]. Multifractal geometry thus offers a way to explain ergodicity-breaking and adaptive aspects of measured behavior [41–45]. If the organism coordinates its degrees of freedom through cascadelike flows (cf. Refs. [1–3]), then the empirical multifractal evidence of nonlinear interactions (i.e., "multifractal nonlinearity") may be uniquely poised to show how [61–66]. A perceptuomotor example of the foregoing may illustrate the explanatory benefits and applied potential of cascade modeling. Manually wielding an unseen object (e.g., with eyes closed, in the dark, or with the hand behind an occluding surface) is sufficient to provide a human participant with an impression of how heavy or how long the object is [67] and providing visual feedback on these perceptual judgments can improve the judgments [68]. Wielding on any trial exhibits fractal structure, and changes in fractality (i.e., multifractality) of this wielding from trial to trial predict individual differences in perceptual responses across repeated trials [69]. Head sway carries similar trial-to-trial variation in fractality predicting the use of visual feedback [60]. Multifractal structure of movement fluctuations across the body and the linear causal models confirm that perceptuomotor performance in such tasks does depend, adapt, and become more accurate through a bodywide network of multifractal flows [57,61,62]. In a more applied vein, understanding these multifractal fluctuations might help to detect disorders in them [70–72] and also provide noninvasive but targeted interventions that could support more accurate perceptuomotor performance [70,73–75]. Multifractal geometries allow us to query the role of multiplicative interactions that enact cascades in coordinating adaptive organismal behavior.

B. The present study: Examining the multifractal nonlinearity of multiplicative and additive cascades incorporating multifractal noise

The present work uses numerical simulations to develop principled expectations for what this empirical multifractal evidence of nonlinearity should look like when we allow cascades to absorb multifractal fluctuations. Specifically, we numerically simulated additive and multiplicative cascades with four types of multifractal noise terms across cells within these cascades: (i) nonlinearly multifractal—multifractal structure with original nonlinear interactions across scales from a cascade process; (ii) linearly multifractal—noise with the same multifractal spectrum width but arising out of purely linear interactions (obtained via the iterative amplitude adjusted wavelet transform of multifractal nonlinearity (IAAWT) [76,77]; (iii) phase-randomized linearity—noise with nonlinear interactions removed that preserved only the multifractal-spectrum width attributable to linear correlations (obtained via the iterative amplitude adjustment Fourier transform (IAAFT) [78,79]; and (iv) shuffled noise that destroyed phase and amplitude spectra, leaving only multifractality due to PDF skew.

We evaluated three specific hypotheses, considering the range of data collection and processing decisions a behavioral scientist might encounter with multifractal analysis. Hypothesis 1 was that multiplicative cascades would promote wider multifractal spectra across progressively more generations—on both the left and right sides of the spectra to increase α at the peak for $q = 0$ (Hypothesis 1a). We hypothesized further that sequential heterogeneity introduced by nonlinear temporal correlations in multifractal noise would make multifractal spectra more asymmetric (Hypothesis 1b). Specifically, we predicted this asymmetry would extend towards the left side, accentuating heterogeneity in large-sized events. We made this prediction while maintaining the evidence-based inference that, as previously found [80], relatively linear correlations would promote the right-side spectrum width. We predicted that multifractal-spectral symmetry might be stronger even for more homogeneous portions of the linearized surrogates. Linearized surrogates from the IAAFT and IAAWT are relatively time symmetric, leading their beginnings and endings to show a transient on either side of their more homogeneous middle [81,82]. Last, we hypothesized that sampling these multifractal noise processes from their beginning or midpoint would change their effects on the resulting multifractal spectra and multifractal nonlinearity, t_{MF} (Hypothesis 1c). Specifically, we predicted that the noise sampled from the more homogeneous middle of the linearized multifractal time series might contribute to cascade dynamics with more symmetric multifractal spectra.

Hypothesis 2 was that multiplicative cascades are more likely to promote "multifractal nonlinearity," defined by t_{MF}, the t-statistic comparing an original cascade time series' multifractal spectrum width $\Delta\alpha_{\mathrm{Orig}}$ to a sample of phase-randomized surrogates time series' multifractal spectrum widths $\Delta\alpha_{\mathrm{Surr}}$ [80]. In keeping with previous simulations [80,83], we expected that, no matter the noise type, multiplicativity rather than additivity would increase the size and

statistical significance of the t_{MF} of simulated time series with progressively more generations.

Furthermore, we expected in Hypothesis 3 that nonlinearly multifractal noise would contribute to the ergodicity breaking of the resulting cascade time series. Because ergodicity guarantees stable averages across time, it depends on Gaussian variance and mixing, that is, homogeneity of a sequential structure consistent with uncorrelated fluctuations [8]. Although multiplicative and additive cascades break ergodicity for different reasons, namely non-Gaussianity and sequential heterogeneity, respectively, multiplicative cascades are more sensitive than additive cascades to the sequential ergodicity-breaking of constituent noise processes [80]. Accordingly, we hypothesized that nonlinearly multifractal and linearly multifractal noises exemplifying sequential heterogeneity would be more likely to accentuate sequence-driven ergodicity breaking in multiplicative cascades than the other multifractal noises.

II. METHODS

A. Generating cascade time series

1. Binomial fracturing and binomial noise terms in prior cascade simulation

Cascades involve an iterative process spanning g generations, where n_g cells in each generation manipulate the proportions $p_{i,j}$ contained within them. Here i ranges from 1 to n_j for generation j less than g. In the subsequent generation $(j+1)$, there are n_c children cells per parent, each inheriting proportions denoted as $p_{i,j+1}$, where i ranges from 1 to n_{j+1}. In binomial cascades, each parent cell distributes proportions to two children cells in the next generation (i.e., $n_c = 2$). As elaborated below, we generated eight distinct types of binomial cascades, half following a multiplicative pattern while the other half adhering to an additive pattern. In multiplicative cascades, the proportions allocated to the n_c children cells result from n_c distinct multiplicative operations governing the distribution of the parent cell's proportion. Conversely, in additive cascades, the proportions are determined by n_c distinct addition operations. Our cascades underwent binomial fracturing at each generation, with binomial noise terms conventionally employed to determine the pairings of children cells (Fig. 1). Instead of applying binomial noise, deterministic weights can be used for any ith parent cell in the jth generation; for instance, the fixed pair of weights, $W_1 = 0.25$ and $W_2 = 0.75$, could be applied consistently to calculate the proportions in the $(2i-1)$th and $2i$th children cells in the $(j+1)$th generation, resulting in $p_{2i-1,j+1} = p_{i,j} \cdot W_1$ and $p_{2i,j+1} = p_{i,j} \cdot W_2$, respectively.

2. Beyond binomial noise terms: Binomial-fracturing cascades with noise terms defined across entire generations to test for effects of length, fGn, and multiplicativity

In this study, our primary objective revolves around preserving the binomial fracturing pattern from parent to offspring cells while introducing a random element to the noise terms, extending beyond the confines of the binomial $(W(1), W(2))$ structure. The pivotal deviation involves generating the cascade time series by introducing noise terms spanning the entire generation. These noise terms exhibited variations in interactivity, ranging from additive to multiplicative, and encompass diverse noise types, including multifractally nonlinear, multifractally linear, phase-randomized, and phase- and amplitude-randomized variations. We can now precisely delineate the eight cascade types we simulated using these terms.

(a) Nonlinearly multifractal noise. We generated multifractally nonlinear noise using an established cascade model [84] that shows the deformation predicted by the log-normal model of Kolmogorov [85] and Obukhov [86]. The numerical procedure for generating a time series from our model unfolds as follows. We generate a stochastic process ξ_i, comprising Gaussian white noise with a zero mean. This process contains 2^m samples, where $i < 2^m$ with m representing the number of cascade steps. In the initial cascade step, denoted as $j = 1$ $(j < m)$, we partition the entire interval into two equal subintervals. Subsequently, we multiply each element ξ_i within these subintervals by random weights defined as $\exp[\omega^{(1)}(k)]$, where k takes on values of 0 and 1. Notably, the $\omega^{(1)}(k)$ values constitute independent Gaussian random variables, each possessing a mean of zero and variance of $\langle \omega^{(1)}(k)^2 \rangle = \lambda_0^2$. As we progress to the subsequent cascade step, designated as $j = 2$, we subdivide each existing subinterval into two equal segments. Here we apply the same random weighting $\exp[\omega^{(1)}(k)]$, with k spanning values from 0 to 3. This process continues iteratively until we have completed the m cascade steps. The resulting time series, denoted as x_i, represents the outcome of this cascade process and is expressed as:

$$x_i = \xi_i \exp\left[\sum_{j=1}^{m} \omega^{(j)}\left(\left\lfloor \frac{i-1}{2^{m-j}} \right\rfloor\right)\right], \tag{1}$$

where $\lfloor \cdot \rfloor$ is the floor function. The random variable x_i is not standardized to simplify the notation. We generated such nonlinearly multifractal noise of length $l = 2^{15}$ (i.e., $m = 15$) with its probability density function (PDF) with variance $\lambda^2 = m\lambda_0^2$ according to the Castaing's equation [87]; we used $\lambda^2 = 0.5$. We used these to obtain the other three noise types, which ultimately were used to generate the random additive and multiplicative cascades subjected to multifractal and ergodicity-breaking analysis to test the above-mentioned hypotheses.

(b) Linearly multifractal noise. To generate a linearly multifractal version of this nonlinearly multifractal noise time series, we used the IAAWT method, as outlined in Refs. [76,77]. In the context of a time series with a length of $l = 2^j$, the IAAWT procedure unfolds as follows:

(i) Execute a dual-tree complex discrete wavelet transform, extracting both amplitudes and phases across all j scales for the complex-valued $w_{j,k}$ with k ranging from 1 to 2^{j-1} at each j;

(ii) Randomly rearrange the original data and employ the dual-tree complex DWT to generate randomized wavelet phases at each scale;

(iii) Generate updated $w_{j,k}$ by merging the initial amplitudes with the randomized phases;

(iv) Continuously iterate through the subsequent steps until convergence is attained:

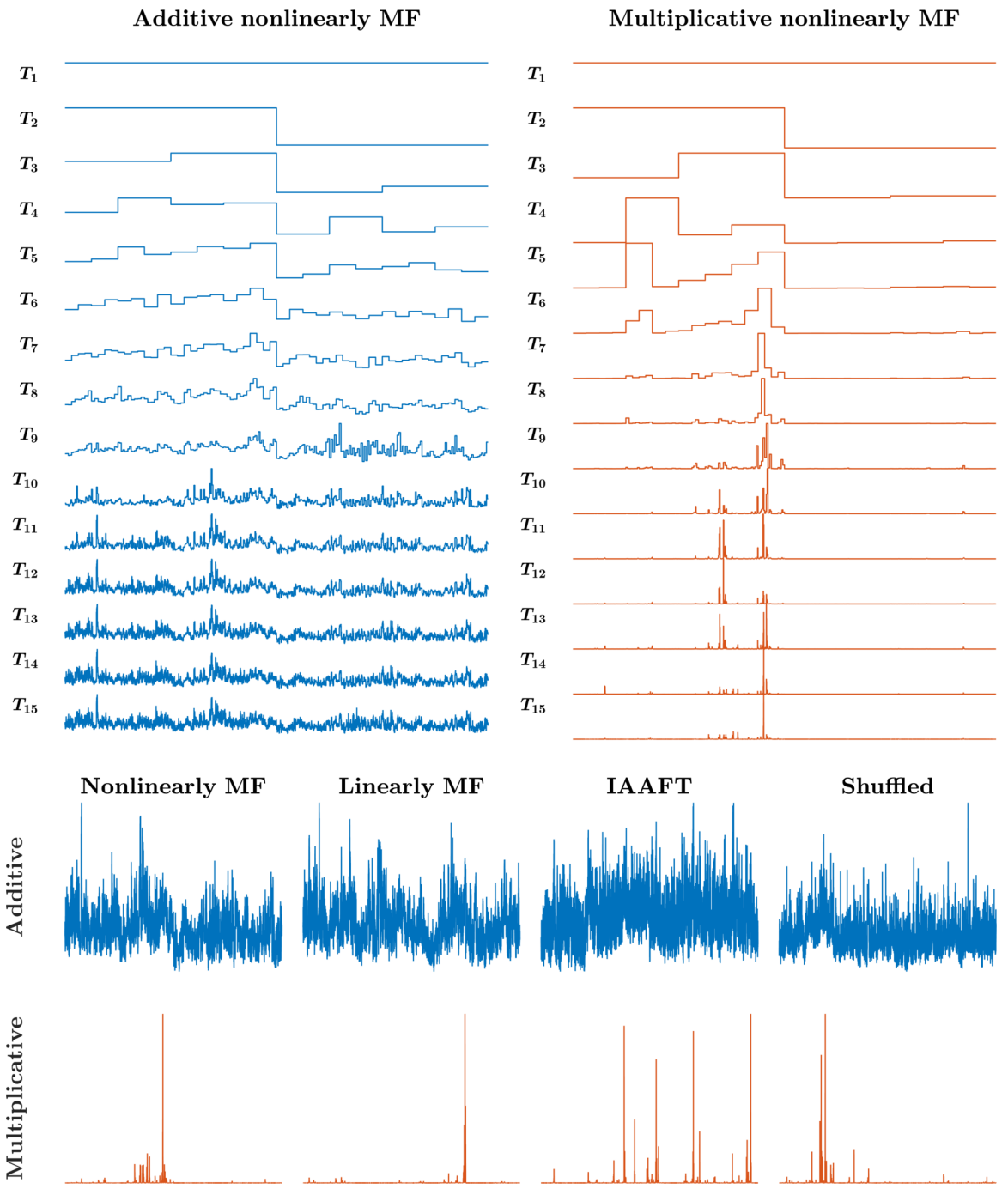

FIG. 1. A binomial additive or multiplicative cascade serves as a mathematical framework for elucidating how the distribution of quantities or events can evolve across increasingly smaller sample sizes and shorter time intervals. In the upper-left quadrant, we observe an additive cascade characterized by multifractal (MF) nonlinear noise terms manifesting across 15 generations of iterative splitting and additive interactions. Meanwhile, in the upper-right quadrant, a multiplicative cascade with MF nonlinear noise terms unfolds over 15 generations, showcasing multiplicative interactions. Each curve has been normalized by its maximum value and vertically shifted by 1 unit to enhance clarity. The lower panel presents a compelling display of both cascade types, exemplifying variations in interactivity that span from additive to multiplicative. Both cascade types encompass various noise types, including nonlinearly multifractal noise, IAAWT-specified linearly multifractal noise retaining both amplitude spectrum and multifractal spectrum width, IAAFT-specific linear noise maintaining only the amplitude spectrum, and random shuffling of the original nonlinearly multifractal noise. Observe the pronounced prevalence of exceedingly large events in multiplicative cascades, not additive cascades.

(a) Execute the inverse wavelet transform to generate a fresh time series, followed by applying the identical amplitude adjustment step in the IAAFT algorithm.

(b) Utilize the dual-tree complex DWT to extract the updated phases and then amalgamate these with the initial amplitudes to produce the most recent $w_{j,k}$.

The IAAWT method retains the original time series' probability distribution while preserving its multifractal structure up to a stringent convergence criterion. We produced 10 IAAWT time series for each original nonlinearly multifractal time series, pinpointing the one that demonstrated the minimal variance in its multifractal spectral width compared to the original nonlinearly multifractal time series.

(c) Phase-randomized, IAAFT noise. To generate a phase-randomized version of this nonlinearly multifractal noise time series, we used the IAAFT method, as outlined in Refs. [78,88]. In the context of a time series $x_t, t = 1, 2, \ldots, N$, the IAAFT procedure unfolds as follows:

(i) Capture and retain the squared amplitudes derived from the discrete Fourier transform of x_t (i.e., $X_f^2 = |\sum_1^N x_t\, e^{i2\pi\, f(t/N)}|^2$);

(ii) Initiate the process by randomly shuffling x_t to yield $x_t^{(j=0)}$;

(iii) Proceed by iteratively executing a power spectrum step followed by a rank-order matching step on $x_t^{(j)}$ in the following manner:

(a) Perform a Fourier transformation on $x_t^{(j)}$ and update the squared amplitudes with X_f^2, keeping the phases intact. Given the initial random sorting, this process conserves the spectrum, albeit with randomized phases. Subsequently, invert the Fourier transformation, restoring the original amplitudes;

(b) Substitute the values within the fresh series $x_t^{(j)}$ with those from x_t through a rank-order matching procedure. While this approach maintains the integrity of the original dataset, it does compromise the precision of spectral matching, thereby elucidating the approximate replication of Fourier amplitudes;

(iv) Continue the process until either the convergence criterion is satisfactorily met or alterations become negligible, thus rendering any reordering of values from the prior iteration unnecessary.

In this way, the PDF of the original time series is preserved precisely, and the Fourier spectrum is approximated to a given error tolerance.

(d) Phase- and amplitude-randomized, shuffled noise. We subjected this nonlinearly multifractal noise time series to shuffling, resulting in a version characterized by randomized phases and amplitudes. Shuffling effectively erases both the phase and amplitude spectra of the time series, thereby nullifying any characteristics associated with the original temporal sequence of values.

Finally, we used these four kinds of noise series to generate the following eight cascade types:

(1) *Additive nonlinearly multifractal*. Noise terms for generation $j+1$ include $x_{2^{j+1}}, x_{2^{j+1}+1}, \ldots, x_{2^{j+2}-1}$ from nonlinearly multifractally noise and the $(2i-1)$th and $2i$th children cells in the $(j+1)$th generation holds proportions $p_i + W_{2i-1,j+1}$ and $p_i + W_{2i,j+1}$, respectively.

(2) *Additive linearly multifractal*. Noise terms for generation $j+1$ include $x_{2^{j+1}}, x_{2^{j+1}+1}, \ldots, x_{2^{j+2}-1}$ from linearly multifractal noise and the $(2i-1)$th and $2i$th children cells in the $(j+1)$th generation holds proportions $p_i + W_{2i-1,j+1}$ and $p_i + W_{2i,j+1}$, respectively.

(3) *Additive IAAFT.* Noise terms for generation $j+1$ include $x_{2^{j+1}}, x_{2^{j+1}+1}, \ldots, x_{2^{j+2}-1}$ from phase-randomized IAAFT noise and the $(2i-1)$th and $2i$th children cells in the $(j+1)$th generation holds proportions $p_i + W_{2i-1,j+1}$ and $p_i + W_{2i,j+1}$, respectively.

(4) *Additive shuffled.* Noise terms for generation $j+1$ include $x_{2^{j+1}}, x_{2^{j+1}+1}, \ldots, x_{2^{j+2}-1}$ from phase- and amplitude-randomized, shuffled, and the $(2i-1)$th and $2i$th children cells in the $(j+1)$th generation holds proportions $p_i + W_{2i-1,j+1}$ and $p_i + W_{2i,j+1}$, respectively.

(5) *Multiplicative nonlinearly multifractal*. Noise terms for generation $j+1$ include $x_{2^{j+1}}, x_{2^{j+1}+1}, \ldots, x_{2^{j+2}-1}$ from nonlinearly multifractal noise and the $(2i-1)$th and $2i$th children cells in the $(j+1)$th generation holds proportions $p_i \cdot W_{2i-1,j+1}$ and $p_i \cdot W_{2i,j+1}$, respectively.

(6) *Multiplicative linearly multifractal*. Noise terms for generation $j+1$ include $x_{2^{j+1}}, x_{2^{j+1}+1}, \ldots, x_{2^{j+2}-1}$ from linearly multifractally noise and the $(2i-1)$th and $2i$th children cells in the $(j+1)$th generation holds proportions $p_i \cdot W_{2i-1,j+1}$ and $p_i \cdot W_{2i,j+1}$, respectively.

(7) *Multiplicative IAAFT.* Noise terms for generation $j+1$ include $x_{2^{j+1}}, x_{2^{j+1}+1}, \ldots, x_{2^{j+2}-1}$ from phase-randomized IAAFT noise and the $(2i-1)$th and $2i$th children cells in the $(j+1)$th generation holds proportions $p_i \cdot W_{2i-1,j+1}$ and $p_i \cdot W_{2i,j+1}$, respectively.

(8) *Multiplicative shuffled.* Noise terms for generation $j+1$ include $x_{2^{j+1}}, x_{2^{j+1}+1}, \ldots, x_{2^{j+2}-1}$ from phase- and amplitude-randomized, shuffled, and the $2(i-1)$th and $2i$th children cells in the $(j+1)$th generation holds proportions $p_i \cdot W_{2i-1,j+1}$ and $p_i \cdot W_{2i,j+1}$, respectively.

To shed light on the underlying factors fueling multifractal nonlinearity within biological and psychological processes, we constructed cascades comprising 2^{14} samples in their 15th and concluding generation. This choice of sample length mirrors the typical empirical time series duration commonly encountered in these domains. To overcome any effects of stochasticity in the generation of these cascades and to ensure robustness in our analysis, we simulated 100 instances for each noise type.

3. Padding cascades with consecutive repetitions of cell values to disentangle generation number from length

Hypothesis 2 suggests that the progressive increase in the number of generations is pivotal in these phenomena. To disentangle the effects of length from those of the number of generations, we extended each generation within the original cascades from the 9th to the 15th generation by padding them with repeated values, ensuring they all shared a uniform length of 2^{14}. We applied a similar technique to the surrogate series to ensure a uniform 2^{14} length. Notably, we only enforced this specific sequence length for the 9th through the 15th generations, as we aimed to maintain the highest confidence in the reliability of the IAAFT surrogates for the original series, particularly for cases where $l \leqslant 2^9$.

B. Multifractal and ergodicity-breaking analysis

We computed key metrics for each cascade instance across generations 9 through 15 to gain insights into its multifractal characteristics. These metrics encompassed the multifractal spectrum width, denoted as $\Delta\alpha$, which we derived employing Chhabra and Jensen's direct method [40]. We also examined the t-statistic, symbolized as t_{MF}, serving as a yardstick for contrasting the multifractal spectrum width $\Delta\alpha_{\mathrm{Orig}}$ of the original series against a set of surrogate samples characterized by their respective multifractal spectrum widths $\Delta\alpha_{\mathrm{Surr}}$. In tandem with these assessments, we assessed ergodicity breaking, employing the Thirumalai-Mountain metric (EB) [89,90]. This metric quantified ergodicity breaking in the original series and extended its reach to randomized shufflings of the same series. It is important to note that while calculating t_{MF} leveraged phase-randomized surrogates to gauge the original series, the evaluation of EB necessitated comparisons with randomized shufflings. This deliberate choice arises because shuffling perturbs linear and nonlinear sources of temporal correlation, contributing to ergodicity breaking.

1. Multifractal analysis

We used Chhabra and Jensen's [40] direct method for qualifying the multifractal structure of each cascade instance across generations 9 through 15. This method estimates multifractal spectrum width $\Delta\alpha$ by sampling a time series $x(t)$ at progressively larger scales using the proportion of signal $P_v(n)$ falling within the vth bin of natural-number scale n as

$$P_v(n) = \frac{\sum_{k=(v-1)n+1}^{v\cdot n} x(k)}{\sum x(t)}, \quad n = \{4, 8, 16, \dots\} < T/8, \tag{2}$$

where $N_n = T/n$. The growth of $P_v(n)$ with n differs depending on the homogeneity of sequence in $x(t)$. For $x(t)$ with homogeneous sequence, as n increases, $P_v(n)$ represents a progressively larger proportion of $x(t)$, such that

$$\sum_{v=1}^{N_n} P_v(n) \propto n^{\alpha}, \tag{3}$$

suggesting a growth of the proportion according to one "singularity" strength α [91]. For $x(t)$ with heterogeneous sequence, multifractal dynamics manifest as multiple singularity strengths, such that

$$P_v(n) \propto n^{\alpha_v}, \tag{4}$$

whereby each vth bin may show a distinct relationship of $P_v(n)$ with n. The width of this singularity spectrum, $\Delta\alpha = (\alpha_{\max} - \alpha_{\min})$, indicates the heterogeneity of these relationships [92,93].

Chhabra and Jensen's [40] method averages across all N_n values of individual bin proportion $P_v(n)$ to estimate $P(n)$ for N_n nonoverlapping n-size bins and transforms them into a "mass" $\mu(q)$ using a q parameter emphasizing higher or lower $P(n)$ for $q > 1$ and $q < 1$, respectively, in the form

$$\mu_v(q, n) = \frac{[P_v(n)]^q}{\sum_{k=1}^{N_n}[P_k(n)]^q}. \tag{5}$$

Then $\alpha(q)$ is the singularity for mass μ-weighted $P(n)$ estimated as

$$\alpha(q) = -\lim_{N_n\to\infty} \frac{1}{\ln N_n} \sum_{v=1}^{N_n} \mu_v(q, n) \ln P_v(n)$$

$$= \lim_{n\to 0} \frac{1}{\ln n} \sum_{v=1}^{N_n} \mu_v(q, n) \ln P_v(n). \tag{6}$$

Equation (6) is the original phrasing from Chhabra and Jensen [40] stated theoretically as a limit. In practice, n is a natural number, and the limit reflects an expectation that the singular dynamics might extend below the sampling rate of a discrete measurement. Each estimated value of $\alpha(q)$ belongs to the multifractal spectrum only when the Shannon entropy of $\mu(q, n)$ scales with n according to the Hausdorff dimension $f(q)$ [40], where

$$f(q) = -\lim_{N_n\to\infty} \frac{1}{\ln N_n} \sum_{v=1}^{N_n} \mu_v(q, n) \ln \mu_v(q, n)$$

$$= \lim_{n\to 0} \frac{1}{\ln n} \sum_{v=1}^{N_n} \mu_v(q, n) \ln \mu_v(q, n). \tag{7}$$

Equations (6) and (7) are the original phrasing from Chhabra and Jensen [40] stated theoretically as a limit, reflecting an expectation that the singular dynamics might extend below the sampling rate of a discrete measurement to the finest of measurable grains. In practical applications of this formalism to discrete series, n is a natural number. We maintain limit notation out of respect for the literature introducing this method and because approximating a continuous variable n can carry more significance when the measurement employs a continuous sampling rate. However, in numerical simulations with arbitrary lengths and discrete outputs, achieving a continuous sampling rate is impractical unless we artificially extend the length of the time series to approximate potentially denser sampling within arbitrarily long intervals. In this scenario, we extend the time series length and conceive each discrete value spanning a shorter scale relative to the overall time series length. We aim for this approach with our "padding" of simulation time series to isolate length effects from generation effects. Following the same rationale, applying discrete n to numerical simulation series approximates continuous n in cases where sampling is more frequent. In this context, the "padded" time series approximates a measurement with a sampling rate finer than the smallest variation in the measurement time series. This approach allows our numerical simulation's natural number n to approximate the empirical measurement case more closely with the continuous sampling rate and continuous n. All measurement time series with reliable sampling rates will themselves reduce to discrete time series, but this was as true for the original demonstrations in Ref. [40]. The limit notion describes a theoretical expectation that the operationalized methodology always aims to estimate across different sampling rates.

For values of q yielding a strong relationship between Eqs. (6) and (7)—in this study, correlation coefficient $r > 0.95$, the parametric curve $\alpha(q)$, $f(q)$ or $(\alpha, f(\alpha))$ constitutes

the multifractal spectrum and $\Delta\alpha$ (i.e., $\alpha_{\max} - \alpha_{\min}$) constitutes the multifractal spectrum width. r determines that only scaling relationships of comparable strength can support the estimation of the multifractal spectrum, whether generated as cascades or surrogates. Using a correlation benchmark aims to operationalize previously raised concerns about misspecifications of the multifractal spectrum [94].

Our next objective was to discern whether a nonzero $\Delta\alpha$ truly signified multifractality arising from intricate nonlinear interactions across various timescales. To achieve this objective, we compared $\Delta\alpha$ values between the original series and 32 IAAFT surrogates [78,79] for each simulated series across generations 9 through 15. IAAFT stands out as a method capable of symmetrically reshuffling the original values around their autoregressive structure. Consequently, it generates surrogates that disentangle the phase ordering of spectral amplitudes within the series while preserving the linear temporal correlations. The one-sample t-statistic, t_{MF}, comes into play by computing the difference between $\Delta\alpha$ for the original series and the corresponding values for the 32 surrogates, which is then divided by the standard error of the spectrum width for these surrogates, facilitating a robust statistical assessment of multifractal nonlinearity.

2. *Justifying our choice of assessing multifractal nonlinearity using the direct method*

We opted for Chhabra and Jensen's [40] direct method over more recent variance-based techniques like detrended fluctuation analysis and wavelet transform modulus maximum [78,95,96]. This decision stems from Chhabra and Jensen's [40] approach, imposing fewer assumptions on the distributions of the measurement time series. While finite variance methods, even when addressing nonstationary time series, assume Gaussian variance beyond presumed stable nonstationarities, often detrended with polynomial functions, such assumptions are seldom guaranteed in measurement time series [97–99]. These assumptions systematically fail in cascade dynamical processes [42]. Moreover, the failure of these distribution assumptions regarding variance across the partition function leads to subsequent failures in the Legendre transformation on which variance-based methods rely [94]. The appeal of Chhabra and Jensen's [40] direct method lies in several aspects. First, while it assumes regular sampling of a continuous process, it employs proportion instead of variance to estimate multifractality directly, bypassing the need for a Legendre transform. Being a nonmicrocanonical method (cf. Ref. [100]), it facilitates stable estimates even for ergodicity-breaking time series, where variance may not be stable, allowing examination of how sample means (in the form of bin proportions) vary over time [101]. Additionally, unlike the Legendre transformation, which estimates both Hausdorff dimension $f(\alpha)$ and singularity strength α as two facets of the same partition function, Chhabra and Jensen's [40] direct method permits independent specification of singularity strengths α and Hausdorff dimension $f(\alpha)$. This enables us to ensure that both quantities reflect stable scaling relationships for each value of q. In essence, Chhabra and Jensen's [40] direct method imposes fewer assumptions on the occasionally ergodicity-breaking series encountered in cascade-driven processes while providing stronger confidence in the estimated multifractal spectrum as a meaningful two-dimensional mathematical structure.

C. Estimating ergodicity breaking parameter for cascade time series

The dimensionless statistic EB, the Thirumalai-Mountain metric, can quantify the degree to which a time series breaks ergodicity [89,90,102] as the variance of sample variance divided by the total-sample squared variance:

$$\mathrm{EB}[x(t)] = \frac{\langle[\overline{\delta^2[x(t)]}]^2\rangle - \langle\overline{\delta^2[x(t)]}\rangle^2}{\langle\overline{\delta^2[x(t)]}\rangle^2}, \tag{8}$$

where $\overline{\delta^2[x(t)]} = \int_0^{t-\Delta}[x(t'+\Delta) - x(t')]^2 dt'/(t-\Delta)$ is the time average mean-squared displacement of the stochastic series $x(t)$ for lag time Δ. Ergodicity with least breaking appears as rapid decay of EB to 0 for progressively larger samples, that is, $\mathrm{EB} \to 0$ as $t \to \infty$. Thus, for Brownian motion $\mathrm{EB}[x(t)] = \frac{4}{3}(\frac{\Delta}{t})$ [4,10]. Slower decay indicates progressively more ergodicity breaking as in systems with less reproducible or representative trajectories, and no decay or convergence to a finite asymptotic value indicates strong ergodicity breaking [103]. $\mathrm{EB}[x(t)]$ thus allows for estimating how much a given time series fulfills ergodic assumptions or breaks ergodicity. Despite the traditional convention of respecting ergodicity as a dichotomy, EB offers a window on how continuous processes can exhibit gradually more or less breaking of ergodicity [41–45]. For instance, Deng and Barkai [103] have shown that for fBm,

$$\mathrm{EB}[x(t)] = \begin{cases} k(H_{\mathrm{fGn}})\frac{\Delta}{t} & 0 < H_{\mathrm{fGn}} < \frac{3}{4} \\ k(H_{\mathrm{fGn}})(\frac{\Delta}{t})^{4-4H_{\mathrm{fGn}}} & \frac{3}{4} < H_{\mathrm{fGn}} < 1. \end{cases} \tag{9}$$

We computed EB for the original and a shuffled version of each cascade instance across generations 9 through 15 (range $= T/8$; lag $\Delta = 2$ samples). The shuffled version allows us to distinguish between two types of ergodicity breaking. Indeed, recent theorizing about ergodicity has elaborated the concept beyond simply the stability of a time-varying process around an ensemble average [8]. This recent theorizing distinguishes that a process can fail to be ergodic if its temporal sequence exhibits heterogeneity even with the stability of time averages around an ensemble average. Hence, whereas traditional ergodicity breaking involves the failure of Gaussian-like stability, ergodicity breaking can also manifest through sequence. The overall height of the EB-vs-t relationship indicates ergodicity breaking due to non-Gaussian PDF [41], and the difference between the decay of the original EB-vs-t curve compared to that for its surrogates indicates ergodicity breaking dependent on sequence [44,103].

III. RESULTS

We analyzed the evolution of multifractality and multifractal nonlinearity over more generations of binomial additive and multiplicative cascades to explore the interplay between these properties and ergodicity breaking within each cascade type. Discussion of the ergodicity-breaking findings will be

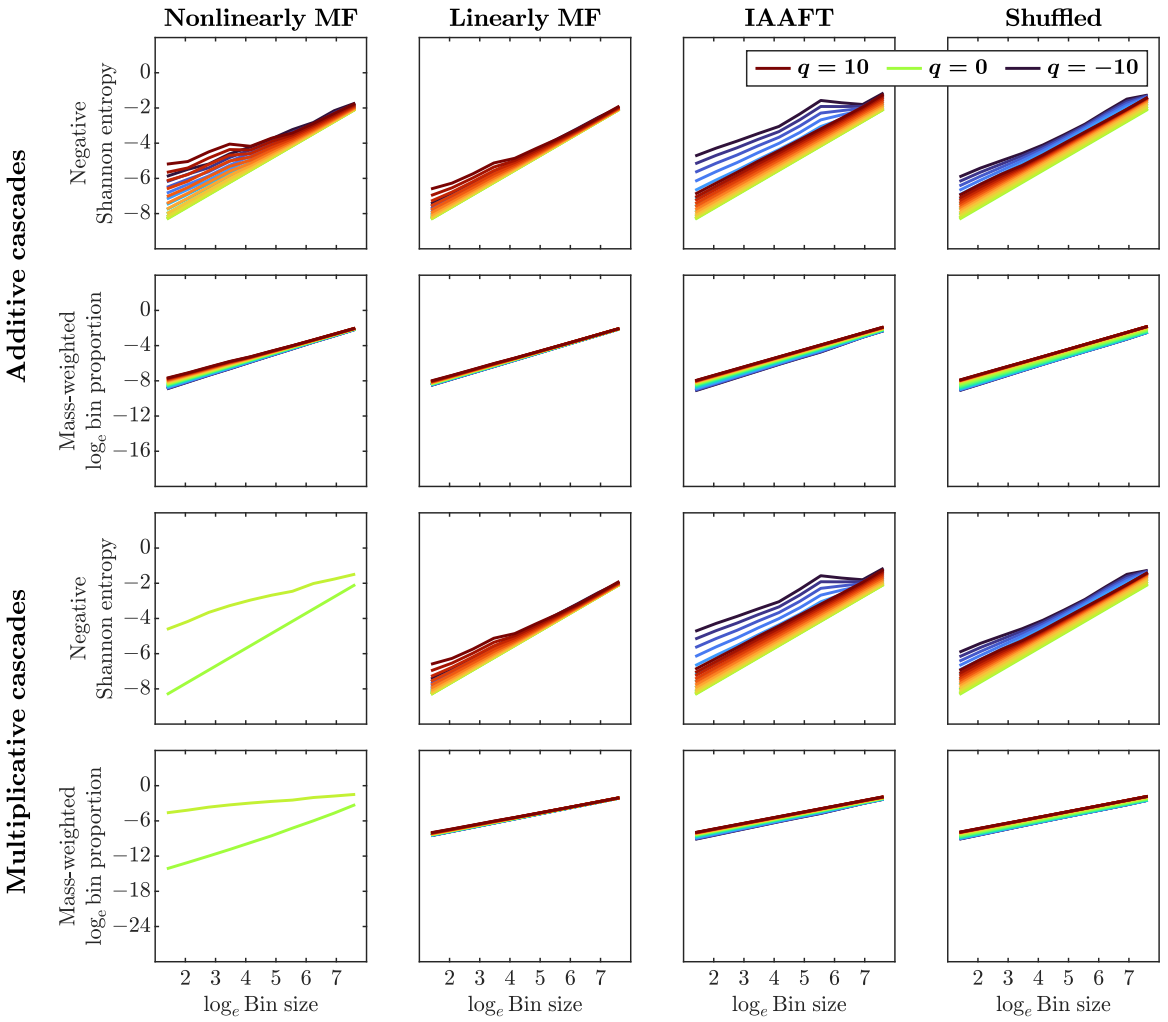

FIG. 2. The scaling relationships underlying Hausdorff dimension $f(q)$ (negative Shannon entropy of bin mass and bin size) and singularity-strength estimates $\alpha(q)$ (mass-weighted average bin proportion and bin size) for the 15th generation of additive and multiplicative cascades for different q, with the cascades involving the application of nonlinearly multifractal noise, IAAWT-specified linearly multifractal noise retaining both amplitude spectrum and multifractal spectrum width, IAAFT-specific linear noise maintaining only the amplitude spectrum, and random shuffling of the original nonlinearly multifractal noise (in the far-left, center-left, center-right, and far-right columns, respectively). We depict only those cases for the range of q for which both $\alpha(q)$ and $f(q)$ describe scaling relationships with $r > 0.95$.

postponed until we present outcomes pertinent to Hypothesis 2.

A. Hypothesis 1: Multiplicative interactions dictate emergent multifractal properties with nonlinearly multifractal noise inducing spectral asymmetry

For now, we detail initial observations of how these multifractal spectra differ across the different types of cascade simulations. Figures 2 and 3 show the scaling relationships for different q and multifractal spectrum for the additive and multiplicative variants of cascades applying each of the four noise types. We ran a linear mixed-effect regression model of three different multifractal spectral attributes to elaborate beyond these cursory portrayals. Our regression model included five covariates:

(1) *Feature,* encoding three types of multifractal-analytical outcomes [104], namely a baseline value of $\alpha_{\max} - \alpha(q = 0)$ (i.e., spectral half-width to the *right* of the peak) and two alternative values of $\alpha(q = 0)$ (i.e., the location of the spectral peak) and $\alpha(q = 0) - \alpha_{\min}(q)$ (spectral half-width to the *left* of the peak).

(2) *Type,* encoding the four types of cascade as described above indicating the kind of multifractal noise, with a baseline value of *nonlinear* and three alternative values *linear*, *IAAFT*, *shuffled*.

(3) *Multiplicativity,* encoding the way that cascade simulations applied noise across generations, with a baseline value of *additive* and alternative value *multiplicative*.

(4) *Generation,* encoding the number of generations from 9 through 15.

(5) *Center,* encoding whether the cascade is sampled from the left of the noise time series (Center = 0) or towards the center of the noise time series (Center = 1).

We used a full-factorial regression model, including the highest-order interaction covariate Feature × Type ×

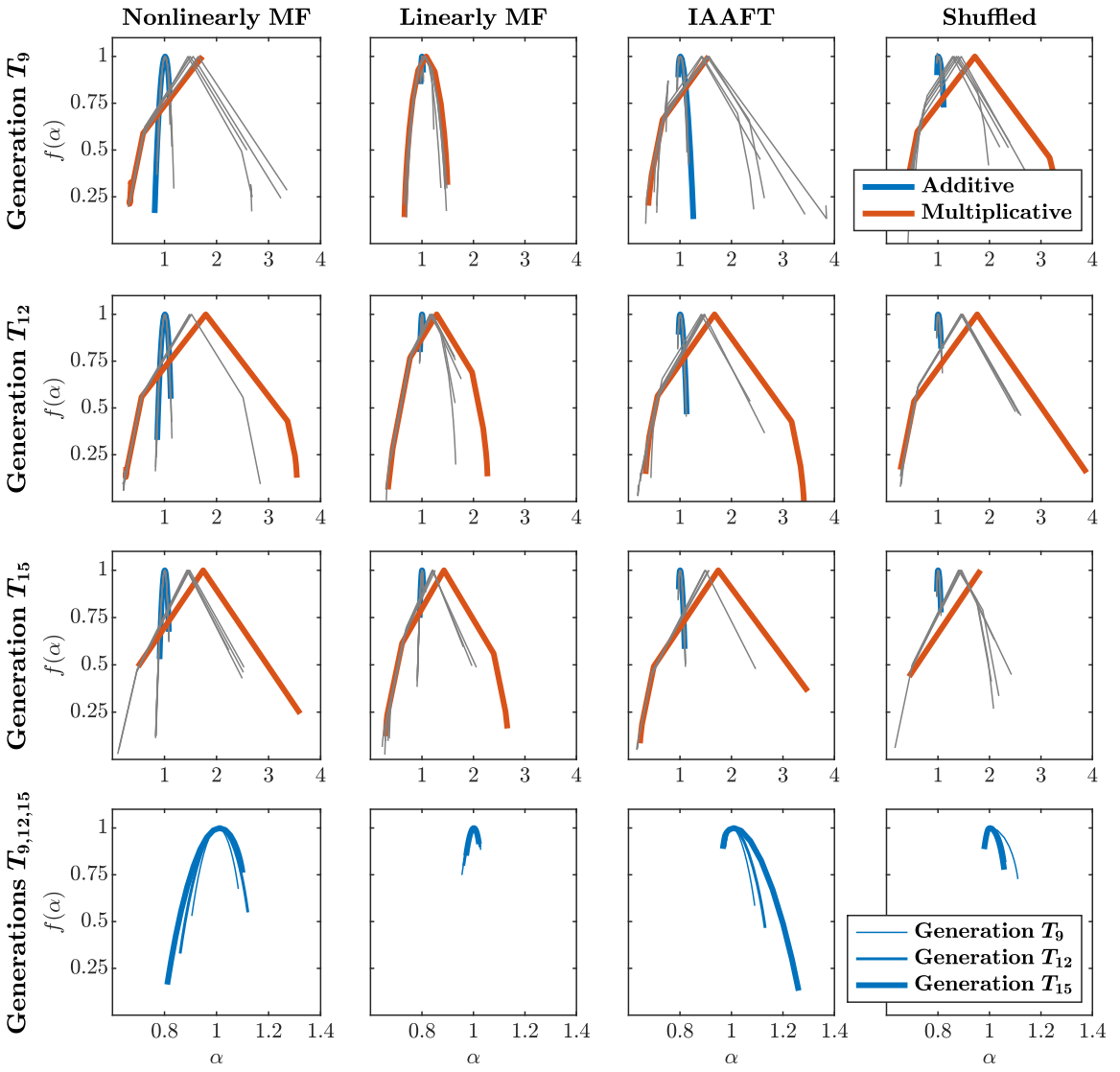

FIG. 3. Representative multifractal spectrum for the four additive and multiplicative cascade types at the 9th, 12th, and 15th generations (top, middle, and bottom, respectively) involving the application of nonlinearly multifractal noise, IAAWT-specified linearly multifractal noise retaining both amplitude spectrum and multifractal spectrum width, IAAFT-specific linear noise maintaining only the amplitude spectrum, and random shuffling of the original nonlinearly multifractal noise (in the far-left, center-left, center-right, and far-right columns, respectively). The colored lines represent the original spectra, while the gray lines depict five representative surrogate spectra generated using the IAAFT method for each original spectrum. Readers may find it challenging to identify the spectra corresponding to additive cascades with IAAFT-specified noise; these spectra are so narrow as to appear at this grain as dots located at roughly $[\alpha = 1, f(\alpha) = 1]$ where the other all-wider additive cascades have their peaks. The bottom panels show additive spectra with an expanded horizontal scale to resolve this issue.

Multiplicative × Generation × Center and all component lower-order interactions and main effects. We used the function `lmer` from the package `lme4` [105] in *R* [106]. We detail the outcomes for each of the three features in the following paragraphs before detailing the outcome for each of our hypotheses. The regression modeling treats the outcome variables as weighted sums of the covariates. It returns B coefficients for each covariate, representing the average change in the outcome variable for a one-unit increase in each corresponding continuous variable. Each coefficient is paired with a standard error SE, reflecting the variance of this average change. We report the estimated coefficients for each covariate that shows a statistically significant effect, with significance determined at the $P < 0.05$ level.

Supporting Hypothesis 1a, the right-side width of the multifractal spectrum, $\alpha_{\max} - \alpha(q = 0)$, grew larger by the ninth generation with multiplicativity and narrowed with progressively more generations. Additive cascades with nonlinearly multifractal noise had nonzero right-side width ($B \pm SE = 1.03 \times 10^{-1} \pm 1.23 \times 10^{-2}$ and $P < 0.0001$). Additive cascades with IAAFT noise reduced this right-side width to almost zero ($B \pm SE = -9.68 \times 10^{-2} \pm 1.73 \times 10^{-2}$ and $P < 0.0001$). In contrast, no other noise had any effect on additive cascades.

Multiplicative cascades with nonlinearly multifractal noise nearly doubled the right-side width at the ninth generation ($B \pm SE = 8.26 \times 10^{-2} \pm 1.73 \times 10^{-2}$ and $P < 0.0001$) but, supporting Hypothesis 1b, also produced almost triple the nonlinearly multifractal noise's rate of narrowing of the right-side width with subsequent generations ($B \pm SE = -1.51 \times 10^{-2} \pm 4.26 \times 10^{-3}$ and $P = 0.0004$). With linearly multifractal and IAAFT noises, the effect of multiplicativity on the 9th-generation right-side width doubled and almost quadrupled, respectively (Bs $= 1.22 \times 10^{-1}$ and 3.00×10^{-1}, SEs $= 2.45 \times 10^{-2}$ and 2.45×10^{-2}, and Ps < 0.0001, respectively). Similarly, linearly multifractal and IAAFT noises also doubled and quadrupled, respectively, multiplicative cascades' narrowing of the right-side width with progressively more generations (Bs $= -1.89 \times 10^{-2}$ and -5.17×10^{-2}, SEs $= 6.03 \times 10^{-3}$ and 6.03×10^{-3}, and Ps $= 0.002$ and < 0.0001, respectively). However, sampling noise processes from the center canceled many effects of these linear noises. The center-sampled IAAFT noise canceled the right-side width diminution for additive cascades ($B \pm SE = 1.08 \times 10^{-1} \pm 2.45 \times 10^{-2}$ and $P < 0.0001$). The center-sampled linearly multifractal and IAAFT noises canceled out the growth of the right-side width on the ninth-generation's right-side width (Bs $= -1.66 \times 10^{-1}$ and -3.28×10^{-1}, SEs $= 3.47 \times 10^{-2}$ and 3.47×10^{-2}, and Ps < 0.0001, respectively). Similarly, sampling the linearly multifractal and IAAFT noises from the center also canceled the otherwise observed doubling and quadrupling, respectively, of multiplicative cascades' narrowing of the right-side width with progressively more generations (Bs $= 3.42 \times 10^{-2}$ and 4.56×10^{-2}, SEs $= 8.52 \times 10^{-3}$ and 8.52×10^{-3}, and Ps < 0.0001, respectively).

In support of Hypothesis 1c, incorporating the center-sampled shuffled noise canceled out the changes on the right-side width of the multifractal spectrum due to nonlinearly multifractal noise, both on the 9th generation and with progressively more generations (Bs $= -6.83 \times 10^{-2}$ and 1.89×10^{-2}, SEs $= 3.47 \times 10^{-2}$and 8.52×10^{-3}, and Ps $= 0.049$ and $= 0.027$, respectively). An alternate regression only on the cascades with shuffled noise revealed no such significant effects of center- versus left-sampling of the noise process at $p < 0.05$. Hence, this finding is largely artifactual of a simultaneous contrast among cascades, the rest of which had expectable trends. Both the linear trends induced by incorporating linearly multifractal and IAAFT noises and the nonlinear trends implicit in nonlinearly multifractal noise. So these effects of the center-sampled shuffled noise indicate that multiplicative cascades with the left-sampled linearly multifractal and IAAFT noises make a stronger contrast with cascades incorporating the left-sampled nonlinearly multifractal noise. The contrast between nonlinearly multifractal noise effects and shuffled noise effects on the right-side width is so small that it only becomes visible when we center-sample the linearly multifractal and IAAFT noises and thus diminish the effect of beginning-transient trends. Hence, multiplicative interactions across progressively more generations produced a greater right-side width and its subsequent narrowing with more generations. They also produced transient trends in progressively more linear, less multifractal noise (i.e., with progressive removal of the phase structure and then removal of the original spectrum width), accentuating both the initial widening and subsequent narrowing with progressively more generations. In brief, linearizing linearly multifractal and IAAFT noises induced a trend at the beginning of the noise process that diminishes the right-side width. If this effect complemented the persisting or growing left-side width, then these effects on the right-side width of the multifractal spectrum could indicate that linear trends across generations of a cascade process could make the spectrum more asymmetric.

The multiplicativity and type of noise at each generation appeared to influence the modal singularity strength, as indicated by the horizontal location of the peak of the multifractal spectrum, $\alpha(q = 0)$. This peak was slightly less than 1 for additive cascades with nonlinearly multifractal noise ($B \pm SE = 9.05 \times 10^{-1} \pm 1.54 \times 10^{-2}$ and $P < 0.0001$) and more so with the left-sampled IAAFT noise ($B \pm SE = 9.00 \times 10^{-2} \pm 2.17 \times 10^{-2}$ and $P < 0.0001$). In support of Hypothesis 1a, it increased as well with multiplicative cascades applying the left-sampled nonlinearly multifractal noise ($B \pm SE = 4.97 \times 10^{-1} \pm 2.17 \times 10^{-2}$ and $P < 0.0001$) and—to a greater degree—the left-sampled shuffled noise ($B \pm SE = 2.07 \times 10^{-1} \pm 3.07 \times 10^{-2}$ and $P < 0.0001$), but it reduced with multiplicative cascades applying the left-sampled linearly multifractal noise ($B \pm SE = -1.57 \times 10^{-1} \pm 3.07 \times 10^{-2}$, and $P < 0.0001$) and the left-sampled IAAFT noise ($B \pm SE = -5.84 \times 10^{-1} \pm 3.07 \times 10^{-2}$ and $P < 0.0001$). Hence, as with the right-side width of the multifractal spectrum, preserving the multifractal spectrum width in the left-sampled linearly multifractal noise helps mitigate the decay of modal singularity strength due to phase randomization. This location of the peak increased with progressively more generations of multiplicative cascades with the left-sampled nonlinearly multifractal noise ($B \pm SE = 3.10 \times 10^{-2} \pm 6.03 \times 10^{-3}$ and $P < 0.0001$), increasing with progressively more generations almost twice as fast with the left-sampled linearly multifractal noise ($B \pm SE = 2.22 \times 10^{-2} \pm 8.52 \times 10^{-3}$ and $P = 0.009$) and more than twice as fast with the left-sampled IAAFT noise ($B \pm SE = 8.37 \times 10^{-2} \pm 8.52 \times 10^{-3}$ and $P < 0.0001$). Hence, multiplicative interactions across progressively more generations counteract the earlier effects of phase randomization, building back the modal singularity strength.

Again, as Hypothesis 1c predicted, linearly multifractal and IAAFT noises canceled out the abovementioned effects from the left-sampled effects. Center-sampling IAAFT noise canceled out the increase in the singularity of the peak in additive cascades ($B \pm SE = -9.97 \times 10^{-2} \pm 3.07 \times 10^{-2}$ and $P = 0.001$), canceled out the reduction in peak singularity for multiplicative cascades ($B \pm SE = 6.70 \times 10^{-1} \pm 4.35 \times 10^{-2}$ and $P < 0.0001$), and canceled out the increase in peak singularity ($B \pm SE = -7.69 \times 10^{-2} \pm 1.21 \times 10^{-2}$ and $P < 0.0001$). Similarly, center-sampling linearly multifractal noise canceled out the reduction in peak singularity for multiplicative cascades ($B \pm SE = 1.82 \times 10^{-1} \pm 4.35 \times 10^{-2}$ and $P < 0.0001$) and canceled out the increase in peak singularity ($B \pm SE = -3.62 \times 10^{-2} \pm 1.21 \times 10^{-2}$ and $P = 0.003$).

With the foregoing narrowing of the right-side width, the peak $\alpha(q = 0)$ value increase goes hand in hand with an extension of the left-side width of the multifractal spectrum. An important point to highlight in support of Hypothesis 1a is that, whereas the peak location increased for one of the additive cascade types, the left-side width changed only for multiplicative cascades. Much like the horizontal location of the multifractal spectrum peak, $\alpha(q = 0)$, the left-side width at the ninth generation increased for multiplicative cascades with nonlinearly multifractal noise ($B \pm SE = 8.49 \times 10^{-1} \pm 2.17 \times 10^{-2}$ and $P < 0.0001$) and even more with shuffled noise ($B \pm SE = 2.51 \times 10^{-1} \pm 3.07 \times 10^{-2}$ and $P < 0.0001$). However, the left-side width increased less for multiplicative cascades with linearly multifractal noise ($B \pm SE = -1.59 \times 10^{-1} \pm 3.07 \times 10^{-2}$ and $P < 0.0001$) and progressively less for multiplicative cascades with IAAFT noise ($B \pm SE = -5.82 \times 10^{-1} \pm 3.07 \times 10^{-2}$ and $P < 0.0001$). Here we see a major difference between the results for the left-side width and those for the prior two features (i.e., the right-side width and the peak). In the prior features, linearly multifractal and IAAFT noise accentuated the effects of nonlinearly multifractal nonlinear noise in multiplicative cascades. However, on the left-side width, linearly multifractal and IAAFT noises act in the opposite direction from nonlinearly multifractal noise. Here we see support again for Hypothesis 1b that nonlinear temporal correlations in multifractal noise promote spectral asymmetry, with a predominance of the left side at the expense of the right-side width—hence, phase-randomization reduces the left-side width. Yet again, even the opposition of these noises to the nonlinearly multifractal case shows a similar buffering of cascades' multifractal spectrum width. Although phase-randomized noise counteracts more of the nonlinearly multifractal noise's effect on the left-side width, phase-randomized noise maintaining the multifractal spectrum width from the nonlinearly multifractal case exerts less of this diminution of the multifractal structure. Beyond the ninth generation, the left-side width increased with progressively more generations for nonlinearly multifractal noise ($B \pm SE = 5.04 \times 10^{-2} \pm 6.03 \times 10^{-3}$ and $P < 0.0001$). This increase was faster—by almost an additional half of the nonlinearly multifractal rate—for multiplicative cascades with linearly multifractal noise ($B \pm SE = 2.20 \times 10^{-2} \pm 8.52 \times 10^{-3}$ and $P = 0.010$), and the left-side width increased at almost double the nonlinearly multifractal rate ($B \pm SE = 8.66 \times 10^{-2} \pm 8.52 \times 10^{-3}$ and $P < 0.0001$). So, again, as with the other two features of the multifractal spectrum, the progressively more multiplicative interactions across generations balance out the effects of the phase-randomized noises, both linearly multifractal and IAAFT noises.

Once more, in support of Hypothesis 1c, center-sampling IAAFT noise and linearly multifractal noise canceled out the effects noted above from the left-sampled effects. Center-sampling IAAFT noise canceled out the reduction in the left-side width for multiplicative cascades ($B \pm SE = 1.79 \times 10^{-1} \pm 4.35 \times 10^{-2}$ and $P < 0.0001$) and canceled out the increase in the left-side width ($B \pm SE = -3.69 \times 10^{-2} \pm 1.21 \times 10^{-2}$ and $P = 0.002$). Similarly, center-sampling linearly multifractal noise canceled out the reduction in the left-side width for multiplicative cascades ($B \pm SE = 7.03 \times 10^{-1} \pm 4.35 \times 10^{-2}$ and $P < 0.0001$) and canceled out the increase in the left-side width ($B \pm SE = -8.22 \times 10^{-2} \pm 1.21 \times 10^{-2}$ and $P < 0.0001$).

B. Hypothesis 2: Multiplicativity amplifies multifractal nonlinearity

Multifractal spectrum width for the original time series ($\Delta\alpha_{\text{Orig}}$) was largely constant across generations 9 through 15 (Figs. 3 and 4, top), while multifractal spectrum widths for the linearly structured IAAFT surrogates ($\Delta\alpha_{\text{Surr}}$) was reduced (Figs. 3 and 4, middle). Specifically, the t-statistic expressing multifractal nonlinearity by comparing $\Delta\alpha_{\text{Orig}}$ and $\Delta\alpha_{\text{Surr}}$—that is, multifractal nonlinearity t_{MF}, grew across progressively more generations, reaching $t_{\text{MF}} = 50$ by the 15th generation (Fig. 4, bottom). Hence, evidence for the cascade process's multifractal nonlinearity becomes clearer as the surrogate-spectrum width narrows with more generations.

To model the change of these quantities, we used a full-factorial regression model, much like that for features above, replacing the covariate *Feature* with an analogous covariate *Outcome* assigned a baseline value of $\Delta\alpha_{\text{Orig}}$ and alternate values $\Delta\alpha_{\text{Surr}}$ and t_{MF}. The highest-order interaction in the regression modeling of these quantities was Outcome × Type × Multiplicative × Generation, and modeling included all component lower-order interactions and main effects. In what follows, we detail the effects of these factors on t_{MF} both in terms of its continuous variation and its more dichotomous status as statistically significant or not, using the functions `lmer` and `glmer` from the package `lme4` [105] in *R* [106].

1. Multiplicative interactions across scales increased the continuous value of t_{MF} except when involving IAAFT noise

The linear regression modeling of continuous t_{MF} had eight significant effects, all referring only to changes in t_{MF}. The general indication was twofold. First, multiplicativity incorporating nonlinearly multifractal noise promoted the growth of t_{MF} across progressively more generations of the cascade. Second, whereas IAAWT-series and shuffled-time-series noises produced no difference in t_{MF} for multiplicative cascades as compared to nonlinearly multifractal noise, multiplicative cascades with IAAFT noise reduced progressively diminished t_{MF} across progressively more generations of the cascade. The sampling issue only appeared in the first nine generations, with left-sampling showing a diminution of t_{MF} in additive cascades and accentuation of t_{MF} in multiplicative cascades.

The results replicated various previous effects [80]. For instance, by the ninth generation, multiplicative cascades initially exhibited smaller t_{MF} ($B \pm SE = -9.16 \times 10^{0} \pm 3.00 \times 10^{0}$ and $P = 2.239 \times 10^{-3}$). Subsequent generations reversed this difference: Additive cascades exhibited significantly lower t_{MF} with progressively more generations ($B \pm SE = -1.90 \times 10^{0} \pm 5.88 \times 10^{-1}$ and $P = 1.247 \times 10^{-3}$), and multiplicative cascades exhibited significantly higher t_{MF} with progressively more generations ($B \pm SE = 7.90 \times 10^{0} \pm 8.31 \times 10^{-1}$ and $P < 0.0001$). The notable exception to this initial finding was a set of cascades with IAAFT noise. Additive cascades with IAAFT noise had dramatically lower t_{MF} on the ninth generation ($B \pm SE = -1.29 \times 10^{1} \pm 3.00 \times 10^{0}$ and $P = 1.700 \times 10^{-5}$), but multiplicative cascades with IAAFT noise had dramatically higher t_{MF}

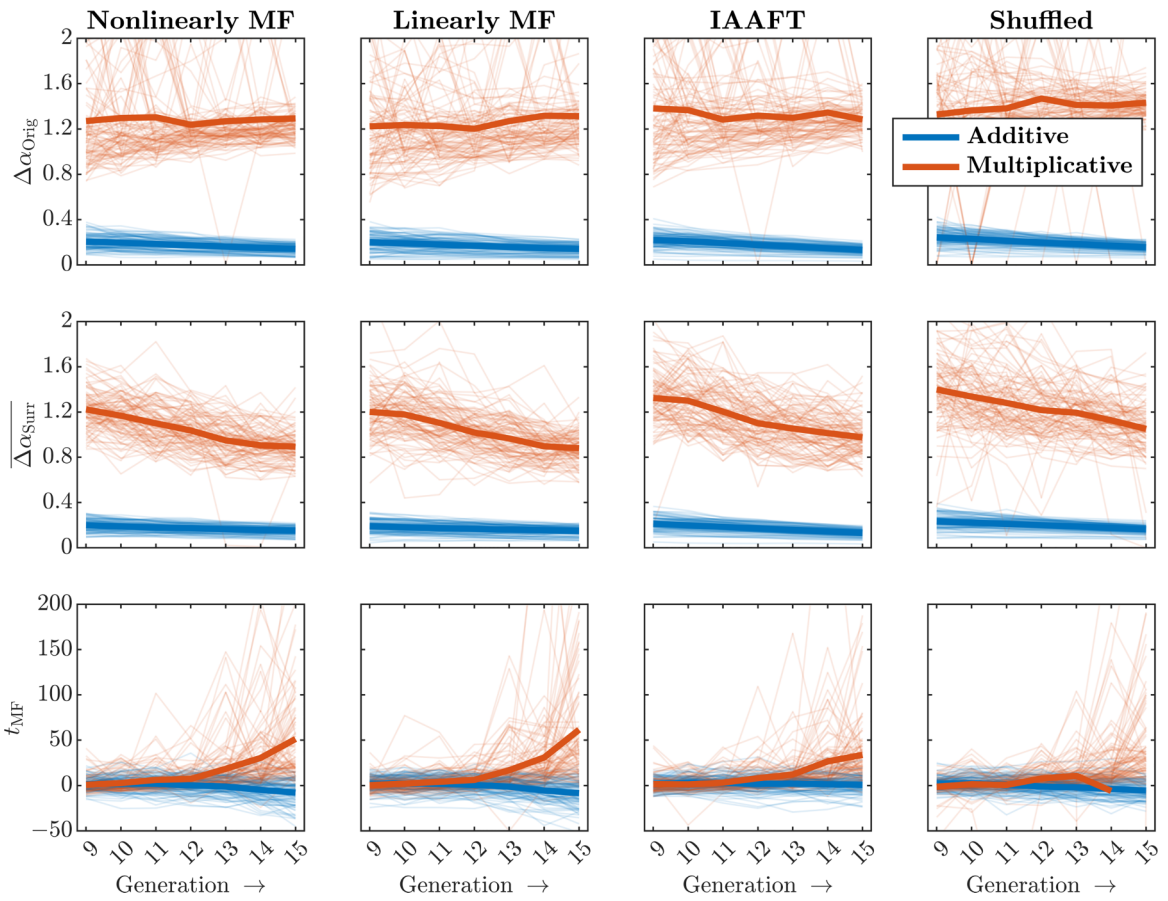

FIG. 4. Multifractal spectral properties of the four additive and multiplicative cascade types across progressively more generations. Multifractal spectrum width for the original cascades $\Delta\alpha_{\mathrm{Orig}}$ (top), multifractal spectrum width for the corresponding 32 IAAFT surrogates $\overline{\Delta\alpha_{\mathrm{Surr}}}$ (middle), and multifractal nonlinearity t_{MF} (bottom) involving the application of nonlinearly multifractal noise, IAAWT-specified linearly multifractal noise retaining both amplitude spectrum and multifractal spectrum, IAAFT-specific linear noise maintaining only the amplitude spectrum, and random shuffling of the original nonlinearly multifractal noise (far-left, center-left, center-right, and far-right, respectively). The bold lines represent the average values derived from $N = 100$ numerical simulations, while the finer lines alongside them portray individual data points within these simulation sets.

on the ninth generation ($B \pm SE = 1.62 \times 10^{1} \pm 24.24 \times 10^{0}$ and $P = 1.290 \times 10^{-4}$). Then multiplicative cascades with IAAFT showed none of the rest of multiplicative cascades' growth of t_{MF} with progressively more generations, instead yielding a diminution of t_{MF} with progressively more generations ($B \pm SE = -2.88 \times 10^{0} \pm 1.18 \times 10^{0}$ and $P = 1.421 \times 10^{-2}$).

The only difference in the effects for cascades with the center-sampled noise was for the IAAFT-noise case. Center-sampling the IAAFT noise canceled out the observed reduction in t_{MF} for additive cascades ($B \pm SE = 1.18 \times 10^{1} \pm 4.24 \times 10^{0}$ and $P = 5.327 \times 10^{-3}$) and canceled out the relative increase of t_{MF} across the nine generations for multiplicative cascades ($B \pm SE = -1.29 \times 10^{1} \pm 4.24 \times 10^{0}$ and $P = 3.129 \times 10^{-3}$). The only feature that persisted when IAAFT noise was sampled from the center was the already-reported diminution of t_{MF} for progressively more generations of multiplicative cascades. To summarize, the effect of the series-beginning trend of IAAFT noise was to reduce and inflate t_{MF} in early generations of additive and multiplicative cascades, respectively. Whether the noise was sampled from the left or the center, incorporating IAAFT noise led multiplicative cascades to *reduce* t_{MF} with progressively more generations.

2. Multiplicative interactions across scales increased the likelihood of statistically significant t_{MF} except when involving IAAFT noise

To model the number of significant positive values of $t_{\mathrm{MF}} > 2.04$, we used a mixed-effect logistic regression with the function `glmer` from the package `lme4` [105] in *R* [106]. Models replicating the same family of higher-order and component lower-order interactions and main effects did not converge. Therefore, we trimmed the model to test only the sum of three main effects and one interaction, namely Type, Multiplicative, Generation, and Type × Generation, and found significant effects.

The pattern of significance we found for explaining positive, significant t_{MF} reflected the same themes from the continuous-valued model of t_{MF}. First, there were lower logarithmic odds for significant t_{MF} ($B \pm SE =$

$-6.36 \times 10^{-1} \pm 1.63 \times 10^{-1}$ and $P < 0.0001$) early on, that is, in the ninth generation of multiplicative cascades. Additive cascades showed a significant reduction in logarithmic odds of a significantly positive t_{MF} with each generation following the ninth generation ($B \pm SE = -3.04 \times 10^{-1} \pm 2.79 \times 10^{-2}$ and $P < 0.0001$). With each generation after the ninth generation, there was a significant increase in the logarithmic odds of a significantly positive t_{MF} for multiplicative cascades ($B \pm SE = 9.77 \times 10^{-1} \pm 4.13 \times 10^{-2}$ and $P < 0.0001$). Last, additive cascades with IAAFT noise showed the lowest logarithmic odds of a significantly positive t_{MF} ($B \pm SE = -1.51 \times 10^{0} \pm 1.86 \times 10^{-1}$ and $P < 0.0001$). Adding multifractal outcomes for the center-sampled cascades with those for the left-sampled cascades led this regression model to fail to converge. This regression model with failed convergence did show that cascades with the center-sampled IAAFT canceled out the left-sampled IAAFT reduction in logarithmic odds of significantly positive t_{MF} ($B \pm SE = 1.85 \times 10^{0} \pm 2.62 \times 10^{-1}$ and $P < 0.0001$). However, running the same regression model on multifractal outcomes for the center-sampled cascades alone revealed that center-sampling did reverse the results uniquely for IAAFT noise while leaving all other effects intact from the left-sampled results. Specifically, only modeling the multifractal outcomes for the center-sampled cascades suggested an increase in logarithmic odds of significantly positive t_{MF} for cascades with the center-sampled IAAFT noise ($B \pm SE = 3.77 \times 10^{-1} \pm 1.86 \times 10^{-1}$ and $P = 0.043$).

We also applied this regression modeling to significantly negative t_{MF} values (i.e., cases with narrower-than-surrogate original multifractal spectrum). The same regression model converged after removing the interaction of Multiplicativity × Generation and considering only the main effects. Hence, we could not replicate the previous finding that multiplicative cascades were more likely to produce significant negative t_{MF} with fewer generations but less likely to produce significant negative t_{MF} with progressively more generations [80]. However, we found in the present case that additive cascades with IAAFT noise had greater logarithmic odds of producing a significantly negative t_{MF} ($B \pm SE = 1.77 \times 10^{0} \pm 1.81 \times 10^{-1}$ and $P < 0.0001$), although progressively more generations of additive cascades reduced the logarithmic odds of a significantly negative t_{MF} ($B \pm SE = -7.06 \times 10^{-2} \pm 1.78 \times 10^{-2}$ and $P < 0.0001$). Across all generations—early or late—multiplicative interactions reduced the logarithmic odds of significant negative t_{MF} ($B \pm SE = -2.49 \times 10^{0} \pm 1.33 \times 10^{-1}$ and $P < 0.0001$). Notably, this effect of generations weakened but failed to—even at the 15th generation—wipe out the logarithmic odds of significant negative t_{MF} for additive cascades with IAAFT noise. On the other hand, the effect of multiplicativity was sufficient to predict that multiplicative cascades with IAAFT noise would have significantly lower logarithmic odds of a significantly negative t_{MF} than additive cascades with IAAFT noise.

3. Disentangling length and generation effects

The foregoing results provide encouraging evidence that multiplicative interactions across progressively more generations within a cascade strengthen multifractal nonlinearity as indexed by both continuous and significantly positive t_{MF}. However, it is worth noting that the canonical binomial-fracturing method of constructing cascades confounds the generation number with the length of the cascade time series. As noted in previous simulation work [80], this confound can be demonstrated in two ways. First, we can take the final generations' resulting cascade time series and submit subsets of those final-generation time series to multifractal analysis and surrogate comparison. For instance, we can draw $2^6, 2^5, 2^4, 2^3, 2^2$, and 2^1 nonoverlapping subsets of varying lengths, including $l = 2^8, 2^9, 2^{10}, 2^{11}, 2^{12}$, and 2^{13}, respectively, from the final-generation time series. However, the drawback of this first method is that the nonoverlapping definition of these subsets underestimates any effect of the abrupt shifts across binomial fracturing. So we can examine progressively longer subsets whose lengths are not explicitly powers of 2. Length dependencies across these nonoverlapping segments within the 15th generation of the cascade model show stable $\Delta\alpha_{Orig}(q)$, decreasing $\Delta\alpha_{Surr}(q)$, and growing t_{MF} (Fig. 5) with longer nonoverlapping subset. Second, we can draw progressively longer subsets anchored on either the first or last values of the final-generation time series. More specifically, we can use natural-number multiples of our segment lengths [e.g., for $j+1$ generation of a cascade, $l = m \cdot 2^{7+s}, m = 1, 2, 3, \ldots, n/2^{7+s}$, where n is the time series length ($= 2^{14}$) and $s \leqslant j - 7$] and anchoring, to begin with, the first value of the series $p_{1,j+1}$ (e.g., spanning $[p_{1,j+1}, p_{2,j+1}, \ldots, p_{m\cdot 2^{7+s},j+1}]$) or to end with the last value of the series (e.g., spanning $[x_{2^j - m\cdot 2^{7+s}+1,j+1}, x_{2^j - m\cdot 2^{7+s}+2,j+1}, \ldots, x_{2^j,j+1}]$). For these overlapping, natural-number-multiple-length subsets of the final time series, the relationships did not depend on whether subsets began from the beginning and grew towards the end of the 15th generation of the cascade time series (Fig. 6) or from the beginning and grew towards the end of the 15th and final generation of the cascade time series (Fig. 7). In both cases of overlapping subsets, $\Delta\alpha_{Orig}(q)$ remained stable, $\Delta\alpha_{Surr}(q)$ reduced, and t_{MF} grew with greater length.

We had previously simulated "padded" versions of cascade time series to break the length-generation confound. Effectively, this strategy ensures that all time series are the same length, and it merely defines the cells of the binomial-fracturing cascade process over progressively fewer nonoverlapping subsets of the same series length. Hence, the length of the series is the same for every generation. In contrast, previously, a parent cell might have given rise to two children's cells in the next generation. This padding entailed that each parent was simply a subset of the series double the length of each child's cell. Another way to think about this procedure is in terms of the MATLAB procedure "repelem" that takes two inputs (a vector a of length n_a and scalar n_b such that n_b/n_a is a natural number) and outputs a new vector b of length $n_a \cdot n_b$ for which each ith element of a becomes the $[(i-1) * n_b/n_a + p]$th values of b, where $p = \{1, 2, 3, \ldots\} \leqslant n_b/n_a$. Removing the "padding" of repeated values is necessary to compute a surrogate for such a series. The repeated values make it all too likely that a phase randomization that preserves the amplitude spectrum for the padded time series would have a comparable multifractal spectrum. However, multifractal analysis could proceed for the padded

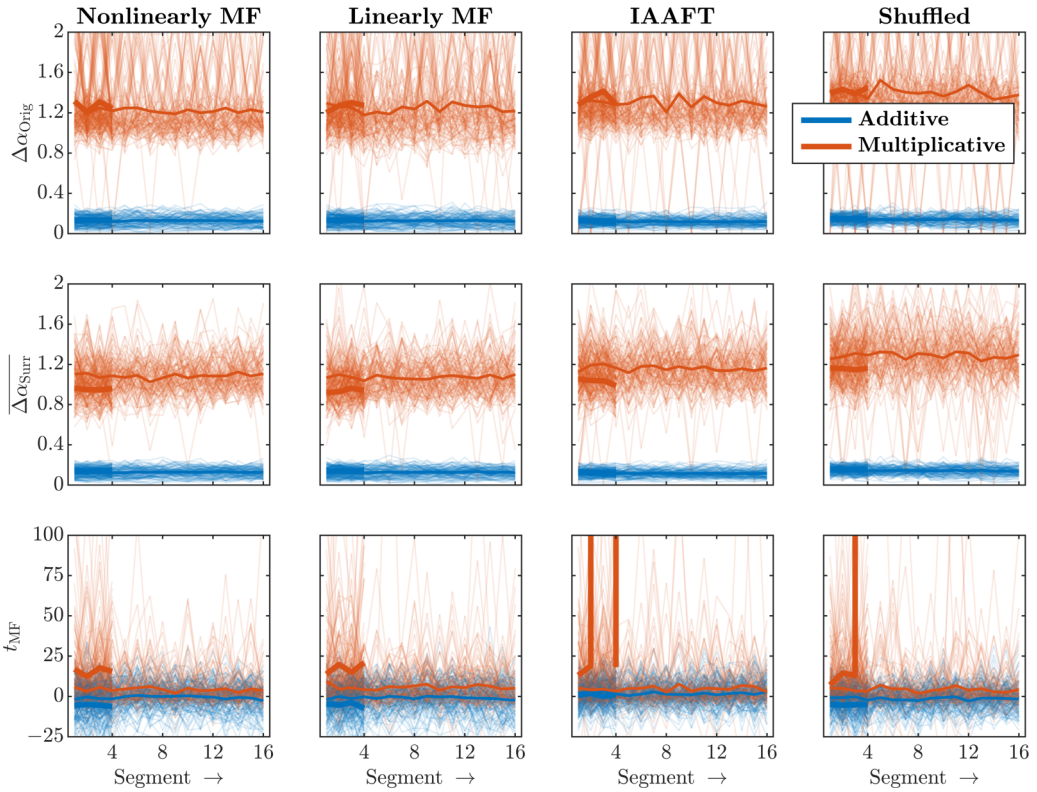

FIG. 5. Multifractal spectral properties of the four additive and multiplicative cascade types across nonoverlapping segments in 15th and final generation. Multifractal spectrum width for the original cascades $\Delta\alpha_{\mathrm{Orig}}$ (top), multifractal spectrum width for the corresponding 32 IAAFT surrogates $\overline{\Delta\alpha_{\mathrm{Surr}}}$ (middle), and multifractal nonlinearity t_{MF} (bottom). Thick and thin lines indicate segments of length $l = 2^{12}$ and 2^{10}, respectively. Each line represents the average values derived from $N = 100$ numerical simulations.

original and surrogate series. This procedure yields equally long time series reflecting different accumulated interactions across timescales. When we thus control for length, the outcome is comparable once more to all foregoing examples: $\Delta\alpha_{\mathrm{Orig}}(q)$ remained stable, decreasing $\Delta\alpha_{\mathrm{Surr}}(q)$, and t_{MF} grew with greater numbers of generations (Fig. 8). Hence, we confirm that the relations we found were not exclusively specific to length.

C. Hypothesis 3: Multifractal heterogeneity in sequence influences ergodicity breaking

Cascades consistently broke ergodicity, a phenomenon detailed in previous work [80]. Interestingly, multiplicative and additive cascades exhibited distinctive forms of ergodicity breaking. Multiplicative cascades, known for generating non-Gaussian PDFs (e.g., Refs. [84,107]), yielded higher intercepts on the EB-vs-t curves compared to their additive counterparts. In stark contrast, additive cascades displayed notably shallow EB-vs-t curves, especially evident as the cascades progress from generations 9 through 15 (Fig. 8, top), emphasizing the robust presence of ergodicity breaking within the additive system. Curiously, the examination of the EB-vs-t curves of additive cascades revealed no distinction between those generated from nonlinearly multifractal and linearly multifractal components.

It is worth noting that the EB-vs-t curves assume flatter profiles for additive cascades constructed from phase-randomized IAAFT noise. Notably, neither the original nor the shuffled multiplicative cascades reach small and diminishing values for the ergodicity breaking factor (EB), as observed in shuffled additive cascades—however, the EB-vs-t curves are visibly shallower for the original time series compared to the shuffled time series, particularly in the cases of multiplicative cascades with nonlinearly multifractal noise and linearly multifractal noise of the same spectrum width. In contrast, the curves are steeper for multiplicative cascades with IAAFT and shuffled noises. This nuanced distinction is evident in the bottom row of Fig. 9, where the original EB-vs-t curves (bolded-line traces) extend beyond two shuffled-time-series curves for multiplicative cascades with nonlinearly and linearly multifractal noises. For multiplicative cascades with IAAFT noise, the EB-vs-t curves barely cross two shuffled-time-series curves. Conversely, multiplicative cascades with shuffled noise exhibit a more linear reduction, crossing only one shuffled-series curve. This pattern holds even for padded "repelem"-type cascades that control for length (Fig. 10).

In summary, the EB-vs-t curves decay more slowly over shorter timescales for cascades with the nonlinearly multifractal and IAAWT-specified linearly multifractal noises. Although multiplicative cascades seem to display weaker ergodicity breaking than additive cascades, the comparable nature of ergodicity breaking across both cascade types suggests that the multifractal spectrum width definitively characterizes the extent of weak ergodicity breaking in the multiplicative case.

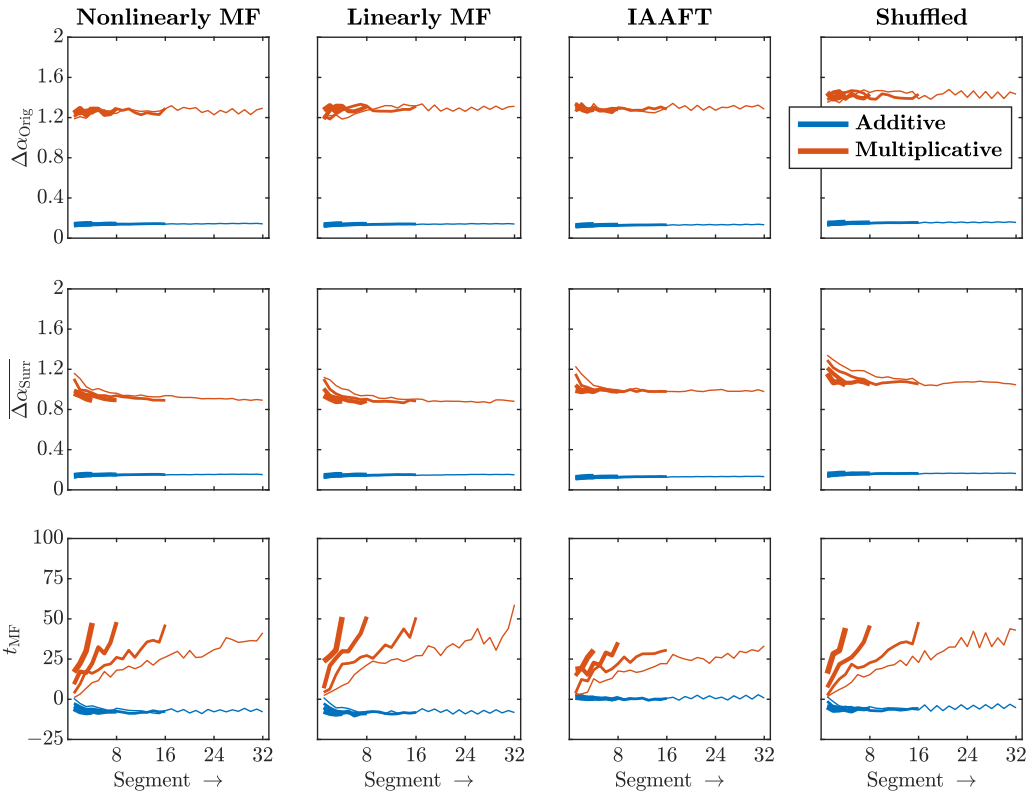

FIG. 6. Multifractal spectral properties of the four additive and multiplicative cascade types across progressively longer segments from the beginning to the end in 15th and final generation. Multifractal spectrum width for the original cascades $\Delta\alpha_{\mathrm{Orig}}$ (top), multifractal spectrum width for the corresponding 32 IAAFT surrogates $\overline{\Delta\alpha_{\mathrm{Surr}}}$ (middle), and multifractal nonlinearity t_{MF} (bottom). The line thickness is reduced progressively from the longest segment length of 2^{12} to 2^{11}, then to 2^{10}, and finally to 2^{9}. Each line represents the average values derived from $N = 100$ numerical simulations.

IV. DISCUSSION

This study examines the outcomes of numerical simulations, underscoring the dominance of multiplicative interactions over the intrinsic nonlinear characteristics of constituent processes. To illuminate this phenomenon, we executed simulations involving cascade time series with component processes operating at disparate timescales. These processes were characterized by four distinct properties: nonlinearly generated multifractality, linearly generated multifractality from constrained phase-randomization (achieved through the IAAWT applied to nonlinearly multifractal), phase-randomized linearity (achieved via the IAAFT applied to nonlinearly multifractal), and phase- and amplitude-randomized (achieved through shuffling of nonlinearly multifractal). Our results establish that the emergent multifractal properties are dictated by the multiplicative interactions among components rather than the intrinsic properties of the component processes themselves. Remarkably, even component processes exhibiting purely linear traits can engender nonlinear interactions across scales when these interactions assume a multiplicative nature. In stark contrast, additive interactions among component processes invariably yield linear outcomes. These findings provide a robust theoretical foundation for current interpretations of multifractal nonlinearity. They firmly situate the origin of multifractal nonlinearity in the realm of multiplicative interactions across scales within biological and psychological processes. We tested three primary hypotheses. First, we posited that multiplicative cascades fostering interactivity across timescales would generate wider multifractal spectra—both on the right and left sides, with peaks corresponding to greater singularity strength α—compared to additive cascades. As a nuance of this first hypothesis, we expected that multiplicative cascades whose cross-scale interactions involved noise with stronger nonlinear temporal correlations would generate multifractal spectra with left-side asymmetry. Second, we anticipated that progressively more generations of multiplicative cascades would yield larger and more statistically significant values of t_{MF}, surpassing the relationships between the length and the number of generations inherent in cascade simulations. Third, we expected that multiplicative cascades would exhibit more pronounced ergodicity breaking based on non-Gaussianity and weaker sequence-driven ergodicity breaking than additive cascades. Throughout, building on our previous discovery that these effects of multiplicative cascade dynamics were more pronounced in cascades incorporating fGn at each generation [80], we explored whether these effects of multiplicativity depended on multifractal noise. Our results validated all these predictions, except that progressively more generations of multiplicative cascades seemed to accentuate a decay of the right-side spectrum width.

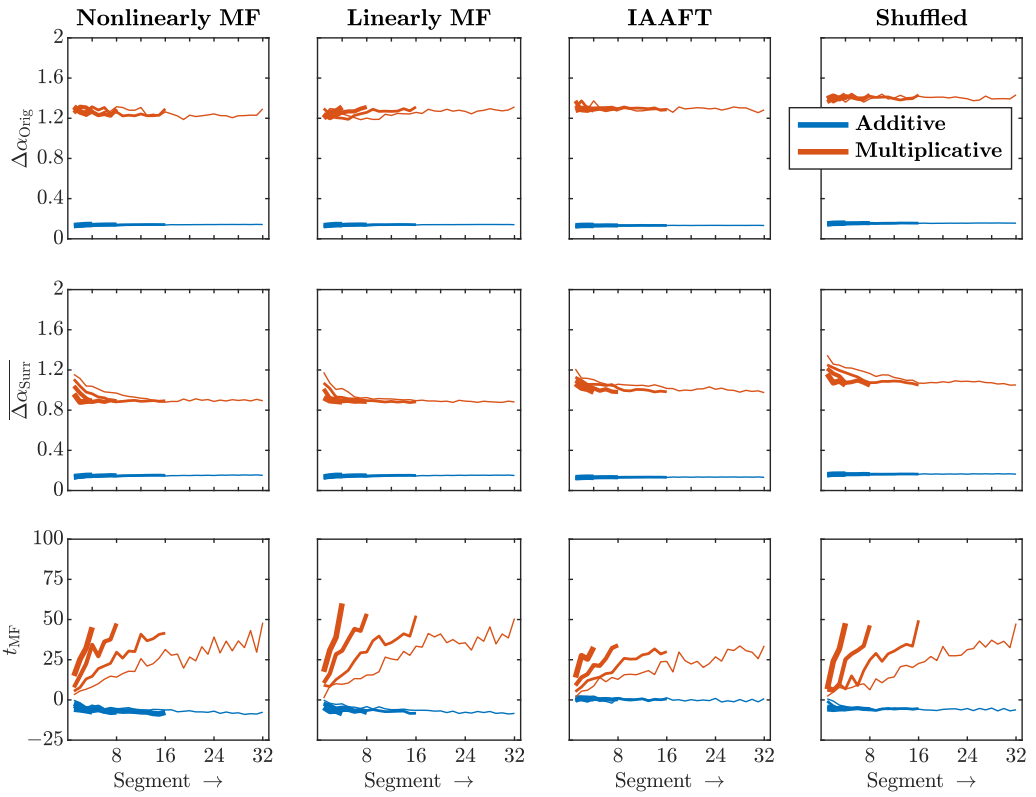

FIG. 7. Multifractal spectral properties of the four additive and multiplicative cascade types across progressively longer segments from the end to the beginning in 15th and final generation. Multifractal spectrum width for the original cascades $\Delta\alpha_{\mathrm{Orig}}$ (top), multifractal spectrum width for the corresponding 32 IAAFT surrogates $\overline{\Delta\alpha_{\mathrm{Surr}}}$ (middle), and multifractal nonlinearity t_{MF} (bottom). The line thickness reduces progressively from the longest segment length of 2^{12} to 2^{11}, then to 2^{10}, and finally to 2^{9}. Each line represents the average values derived from $N = 100$ numerical simulations.

A. Multifractal noise with nonlinear temporal correlations and with linear transients each led multiplicative cascades to promote left-side asymmetry in multifractal spectra

Incorporating multifractal noise processes into multiplicative cascades resulted in multifractal spectra characterized by a broader left side and a more singular peak [i.e., exhibiting a higher $\alpha(q = 0)$]—more asymmetric than previous findings involving monofractal fGn in multiplicative cascades. The width of the multifractal spectrum on the right side aligned with prior work when multifractal noise was introduced, resembling outcomes observed with both additive and multiplicative cascades utilizing additive white Gaussian noise ($awGn$) but not with fGn [80]. Although additive cascades progressively narrowed the right-side width of the multifractal spectrum with progressively more generations, multiplicative cascades initially expanded this width at the ninth generation. These novel outcomes suggest that the application of nonlinearly multifractal noise or phase-randomized multifractal IAAFT noise in early generations can either enhance or diminish, respectively, the heterogeneity represented by small fluctuations on the right side of the multifractal spectrum. Departing from our previous work [80,83], multifractal noises generally reduced the right-side width of the multifractal spectrum, with two nuances: First, multiplicative cascades with nonlinearly multifractal noise narrowed the right-side width with progressively more generations, and secondly, phase-randomized multifractal noises increased the ninth generation's right-side width and accentuated its narrowing, particularly with IAAFT noise compared to the nonlinear case. Confirming previous findings that linearity undermines small-fluctuation heterogeneity [80,83], our results indicate that preserving the original multifractal spectrum width likely maintains small-fluctuation heterogeneity. Furthermore, multiplicative cascades, especially with monofractal fGn, may be more adept at sustaining greater right-side spectrum width across generations. The observed small-size heterogeneity may be attributed to the ergodicity-breaking capacity of fGn and the ability of multiplicative interactions across timescales to translate these effects into heterogeneous sequences within small-sized fluctuations. Likewise, preserving the multifractal spectrum width for noise applied at each generation reinforces cascades with more robust multifractal spectrum widths, a factor not contributing in the case of additive cascades.

This study also reveals how asymmetric multifractal spectra can indicate sensitivity to progressively linearized multifractal noise trends. Despite the initial generations featuring only a handful of children (e.g., 2, 4, 8, and 16 in the first four generations), the expanding pool of offspring in later generations amplifies the influence of diverse multifractal noises on the resulting multifractal structure. The robust time-symmetry of IAAFT noise exerts a profound impact, narrowing both sides of the multifractal spectrum. Transient

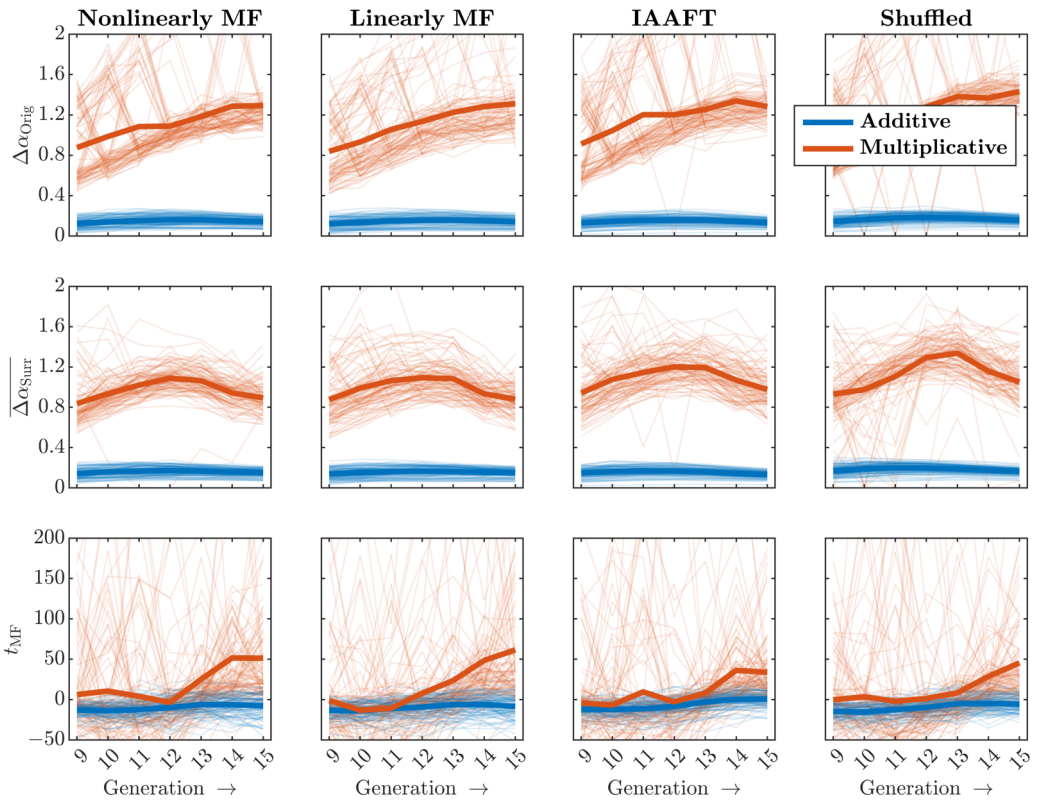

FIG. 8. Multifractal spectral properties of the four additive and multiplicative cascade types across progressively more generations after controlling for length. Multifractal spectrum width for the original cascades $\Delta\alpha_{\mathrm{Orig}}$ (top), multifractal spectrum width for the corresponding 32 IAAFT surrogates $\overline{\Delta\alpha_{\mathrm{Surr}}}$ (middle), and multifractal nonlinearity t_{MF} (bottom). To ensure consistent length across generations, time series were padded with consecutive repetitions of individual-cell values for 9th through 15th generations 64, 32, 16, 8, 4, 2, and 1 times, respectively. The bold lines represent the average values derived from $N = 100$ numerical simulations, while the finer lines alongside them portray individual data points within these simulation sets.

trends at the onset of IAAWT noise also lead to a similar constriction in the resulting cascades' multifractal spectra. This observation is intriguing, considering that IAAWT noise represents a linearization that alters the original sequence while retaining the same multifractal spectrum–a constrained form of phase randomization [108]. Even this constrained phase randomization proves sufficient to generate transients that multiplicative cascades manifest through substantial alterations in the multifractal spectrum. Shuffled multifractal noise exhibits no statistically discernible effects until all these noise processes are sampled from the center. In this scenario, cascades involving the two linearizations of multifractal noise (IAAFT and IAAWT) exhibit the weakest trends, displaying minimal deviation from the nonlinearly multifractal noise. Within these conditions, multiplicative cascades with shuffled multifractal noise showcase their ability to maintain the right-side width. In contrast, multiplicative cascades incorporating nonlinearly multifractal noise yield more asymmetric multifractal spectra with broader left sides. Meanwhile, even when the center of IAAFT processes is sampled, multiplicative cascades with IAAFT noise lead to a progressive reduction of t_{MF} in subsequent generations.

To summarize the effects on spectral features, multifractal noise leads to progressively more asymmetric multifractal spectra with greater left-size width, and this asymmetry grew with progressively more generations for nonlinearly multifractal noise and the left-sampled linear surrogates of multifractal noise. Hence, incorporating multifractal noise can skew the multifractal spectrum of the resulting cascades even with nonlinear temporal correlations in the noise, and linear trends in the noise process unfolding across each generation might accentuate that skewness. So when behavioral and biological sciences find asymmetric multifractal spectra for any single observable, important questions to explore involve (i) whether the observable is receiving multifractal noise from a component process, (ii) whether there are nonlinear and linear sources of such noise, and (iii) whether the linear components of this multifractal noise are in full swing or just beginning to participate in cascadelike relationships across the organism's degrees of freedom. It would also be important to consider how initiating a linear constraint on multifractal noise on the organism's other degrees of freedom might induce a transient asymmetry in the resulting multifractal spectra.

B. Multiplicative cascades promoted greater multifractal nonlinearity t_{MF} except with IAAFT noise

We observed intriguing patterns in the emergence of multifractal nonlinearity across generations. Notably, progressively later generations exhibited a higher value of t_{MF} when comparing the original multifractal spectrum with the spectrum of linear surrogates. This finding aligns with the previous

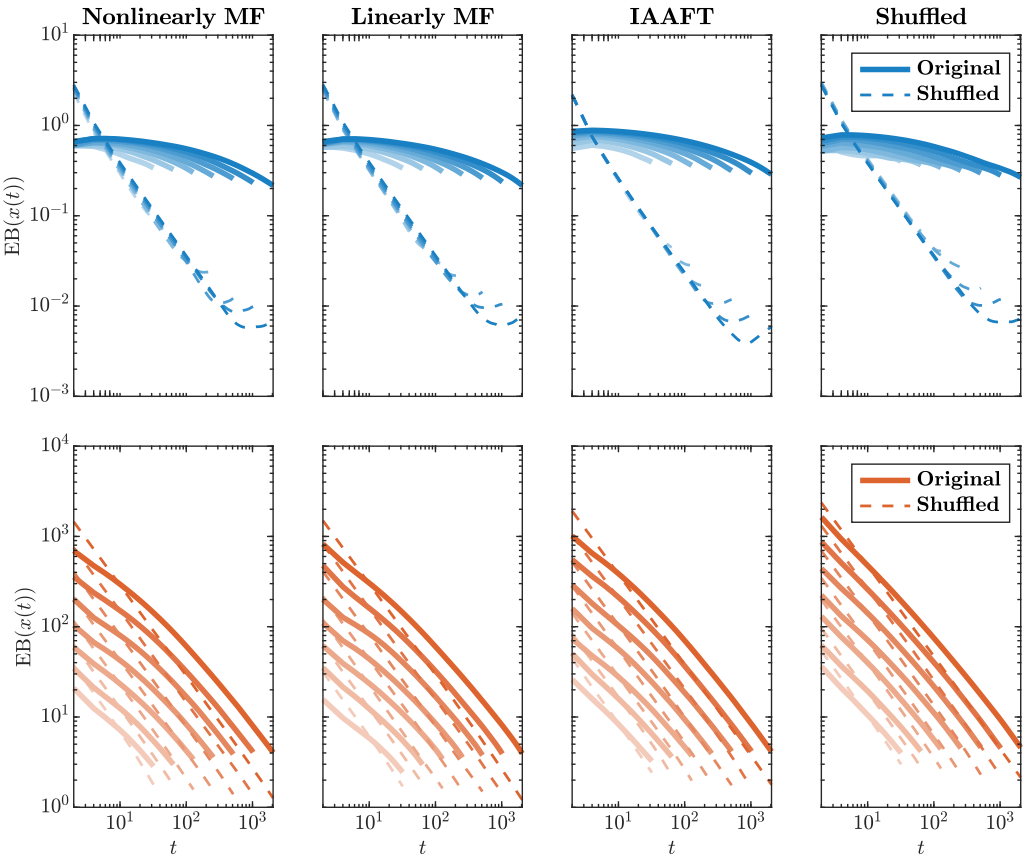

FIG. 9. Ergodicity breaking in the four additive (top) and multiplicative (bottom) cascade types across progressively more generations. This phenomenon is quantified using the ergodicity breaking factor EB[$x(t)$] (lag $\Delta = 2$ samples). The traces progressively deepen in color from 9 through generation 15. Notably, the time series length experiences exponential growth across these generations—$2^8, 2^9, 2^{10}, 2^{11}, 2^{12}, 2^{13}$, and 2^{14} for the 9th through 15th generation, respectively. Each line represents the average values derived from $N = 100$ numerical simulations.

empirical work that interprets increased multifractal nonlinearity as indicative of more intricate interaction-driven dynamics supporting perception and action (see Ref. [65] for review). As the data's sampling duration increased, the growth in multifractal nonlinearity became apparent, providing more robust evidence of nonlinear interactions across scales via IAAFT surrogate comparison, suggesting that nonlinear evidence of cross-scale interactions intensifies with the time series length. Importantly, the independence of multifractality from specific sampling times enhances its reliability as an empirical technique. Multifractal nonlinearity remains constant within a data segment sampled for a specific duration, implying that any chunk of data can represent the entire process, provided the sampling length remains consistent across repeated sampling or comparisons across groups or conditions. Understanding that subsequent events cannot retroactively change the reality of prior evolution in a physical system underscores the significance of consistent interpretation, particularly when analyzing extended datasets. The consistent multifractal nonlinearity across same-length chunks reinforces this point, particularly in the context of multiplicative interactions, supporting our central finding on the pivotal role of such interactions in shaping emergent multifractal properties. Center-sampling only nullified IAAFT's effects on additive cascade t_{MF} and early-generation t_{MF} in multiplicative cascades. Regardless of controlling for transient trends at the beginning of IAAFT noise, multiplicative cascades with IAAFT noise consistently exhibited smaller and less often significant values of t_{MF}. Hence, the asymmetry of multifractal spectra due to all but shuffled-noise multiplicative cascades does not alter the outcome of most multiplicative cascades' multifractal nonlinearity. Comparing the entire cascade time series to its own IAAFT surrogates allowed controlling for many linear factors in the left-sampled noises. Whether sampled from the left or the center of the noise process, IAAFT noise consistently prevented multiplicative cascades from promoting multifractal nonlinearity across generations.

C. Noise with greater multifractal spectrum width contributed to stronger sequence-dependent ergodicity breaking in multiplicative cascades

Finally, our findings regarding ergodicity breaking are particularly thought-provoking. They add confirmatory evidence supporting both the previous theorizing that ergodicity breaking might stem from the sequential structure as well as from the failures of processes to stabilize around Gaussian mean [8] *and* the more recent evidence that additive and multiplicative cascades distinctly promote the former and latter

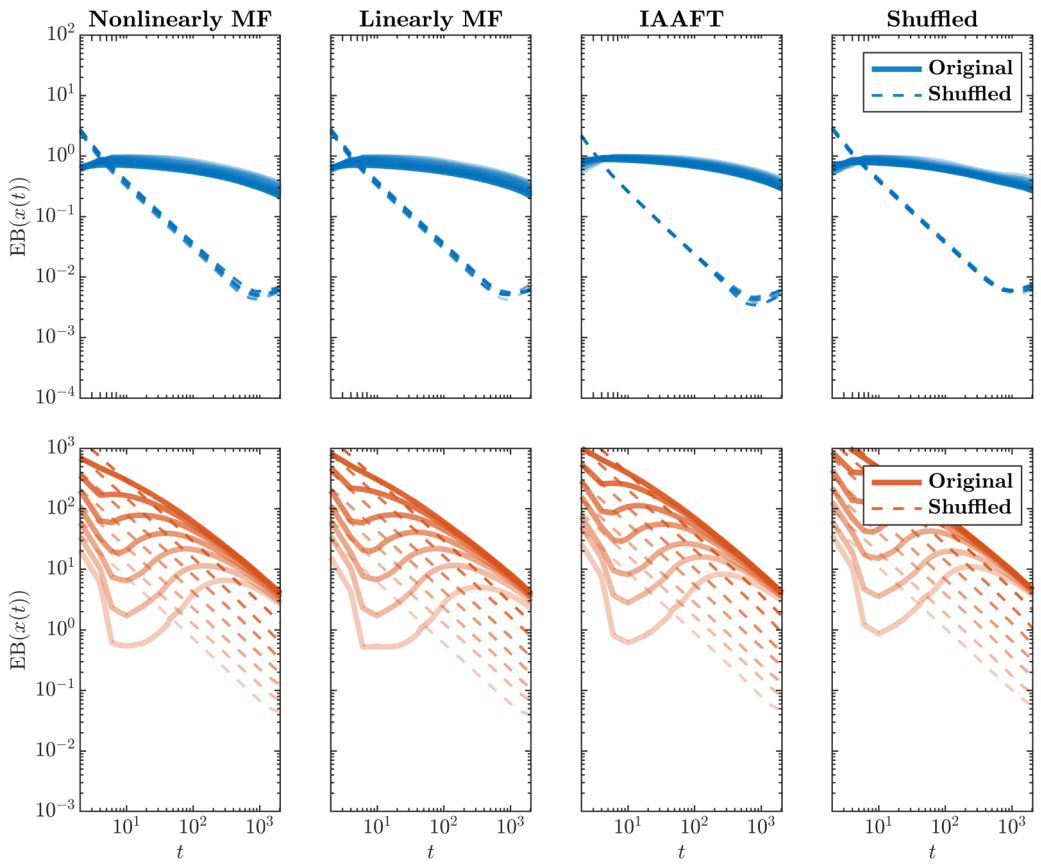

FIG. 10. Ergodicity breaking in the four additive (top) and multiplicative (bottom) cascade types across progressively more generations after controlling for length. This phenomenon is quantified using the ergodicity breaking factor EB[$x(t)$] (lag $\Delta = 2$ samples). The traces progressively deepen in color from 9 through generation 15. To ensure consistent length across generations, time series were padded with consecutive repetitions of individual-cell values for the 9th through 15th generations 64, 32, 16, 8, 4, 2, and 1 times, respectively. Each line represents the average values derived from $N = 100$ numerical simulations.

sources, respectively [80]. We found that additivity promoted sequence-driven ergodicity breaking, as in the case of the linear process *fGn* showing strong ergodicity breaking with greater temporal correlations [103]. We also found that multiplicative cascades showed less sequence-driven ergodicity breaking but greater ergodicity breaking due to non-Gaussian PDF. Again, as in Ref. [80], noise type affected sequence-driven ergodicity-breaking that depended on multiplicativity: the entailment of more homogeneous, more time-symmetric temporal structure in the IAAFT-noise promoted sequence-driven ergodicity breaking in additive cascades, but the wide multifractal spectrum in nonlinearly multifractal noise and its preservation in the linear multifractal noise served to strengthen sequence-driven ergodicity breaking in multiplicative cascades.

Hence, the assessment of ergodic properties remains a pertinent endeavor when modeling biological and psychological processes [41–45,73]. And it now appears consistently that both the mathematical relationship across generations (i.e., multiplications or additions) and the temporal structure in the noise implicated in the cascade process (e.g., nonlinearly multifractal, IAAWT, IAAFT, or shuffled) could each play a part in determining the ergodicity-breaking properties of our raw empirical measurements. Beyond replicating this point from our previous simulation work [80], an intriguing implication of the present findings is that IAAFT noise can provoke strong sequence-driven ergodicity breaking in additive cascades but diminish it in multiplicative cascades. A complementary intriguing implication is that a wider multifractal spectrum appears to promote sequence-driven ergodicity breaking, and the comparable ergodicity-breaking results for multiplicative cascades with nonlinearly multifractal noise and IAAWT noise suggests that nonlinear temporal correlations might not themselves be necessary for sequence-dependent ergodicity breaking. Then again, the contrast of results between cascades with nonlinearly multifractal noise and cascades with IAAFT noise suggests that nonlinear temporal correlations certainly suffice to produce a difference in ergodicity-breaking. Although the failure of mixing (i.e., the linear correlations in IAAFT noise) is sufficient for sequence-driven ergodicity breaking in additive cascades, the greater multifractal spectra for cascades with nonlinearly multifractal noise entail *variety* in the failure of mixing. Previous work had shown that multiplicative cascades with nonmixing *fGn* indeed showed this greater sequence-dependent ergodicity breaking [80]; now we learn from the present results that multiplicative cascades can show greater sequence-dependent ergodicity with greater varieties in failure of mixing. In summary, we conclude that multiplicative cascades might protect against sequence-dependent ergodicity breaking, bringing

relative stability to the cascade outcome precisely when the underlying noise process shows the least variety in its failure of mixing. The same multiplicative cascades appear to unleash relatively more sequence-dependent ergodicity breaking when the underlying noise processes are more variable in their failure of mixing.

D. Conclusion and future directions

We have shown in this simulation work that multifractal formalisms represent a robust approach for evaluating whether fluctuations in empirical time series indicate multiplicative interactions among component processes operating across various scales and in various parts of an extended system. Previous work investigating cascade-driven simulations has traditionally only addressed isolated cascade processes, essentially isolating the parameters of a single cascade and confirming which range of parameters could produce specific ranges of fractal and multifractal outcomes. This work has been crucial for all empirical work considering any observable that may embody a single cascade process. Simulation work with single cascades provides an ample testing ground for exploring why and under what constraints we should expect multifractal outcomes with or without sequence-driven ergodicity breaking—but only in single or isolated degrees of freedom. So long as we hope for cascade-dynamical modeling to speak to organism-wide interactivities, the next crucial step in cascade modeling may be to derive valid theoretical predictions for cascades that are not simply producing multifractal structure but incorporating different forms of multifractal noise as well. The present results provide new perspectives for interpreting how asymmetric multifractal spectra in single observables might reflect multiplicative cascades operating on multifractal noise absorbed elsewhere in the organism or task context. This theoretical work allows asking more subtle questions about the proposed linearity or nonlinearity implicit in multifractal fluctuations endogenous to the organism (e.g., Refs. [61,62]) or in exogenous multifractal stimulation from the task context (e.g., Refs. [70,73–75]).

This proposed direction for theoretical work is decidedly not a program of building multifractal noise to provide a "turtles all the way down" explanation of the origin of multifractal structure in biological and psychological measurements. First, we do not expect that cascade dynamics should be purely transparent to multifractal perturbation—that is, cascade dynamics themselves may be a fundamental mechanism sufficient to produce multifractal structure, and cascade dynamics is a compelling mechanism because cascadelike fracturing is not in and of itself a multifractal mechanism. In other words, cascades constitute minimally only one straightforward route for producing multifractal structure, and there is nothing inherently multifractal about the repetition of biased splitting of proportions in parent cells [92]. Second, we do not aim to re-present long-understood rules of superposition by which adding one fractal signal to another might produce a new signal of superposed fractality [109], and the present work is also not simply adding one multifractal time series to another multifractal time series of comparable length. Beyond what previous work has shown about potentially multifractal or nonmultifractal routes to multifractal results, we can point to the present results as evidence of the diverse effects of incorporating multifractal noise. Indeed, the capacity for zero and (significantly) negative t_{MF} in additive cascades and even multiplicative cascades with IAAFT noise suggests that cascades chart many routes towards nonmultifractal outcomes. While it may not seem significant at first glance, IAAFT noise consistently demonstrated a notable reduction in the multifractal spectrum width compared to the nonlinearly multifractal noise. However, the persistence of a residual nonzero multifractal spectrum width due to the PDF skewness technically qualifies IAAFT noise as multifractal. Furthermore, our observations reveal a noteworthy phenomenon: numerous additive cascades featuring multifractal noise may present only scant evidence of multifractal structure, as exemplified by the subtle traces in the *blue lines* across all *top-row panels* in Figs. 4–7. Consequently, there is no guarantee that cascades consistently yield compelling evidence of multifractality. Similarly, no categorical assurance suggests that we should exclusively expect multifractal structure from cascades generated by applying multiple generations of multifractal noise.

Instead, cascades that incorporate multifractal noise open up a field of theoretical inquiry that paves a path towards scaling a multifractal model of biological and psychological processes up from single observables to an entire organism—that path that network science has already begun to hint at [110]. The present exploration of cascades with multifractal noise is an early step in learning how to interpret our single observables' multifractality better. The present work does not give indicators of network topology; instead, it offers a view of how classic categories of cascades (i.e., additive and multiplicative) react to and involve multifractal noise that might spread through the system from spatiotemporally neighboring points of cascade dynamics. This work informs this line of theoretical inquiry by indicating that the mathematical form of cascade dynamics (i.e., additive or multiplicative) radically changes the effect of the simulated observable absorbing multifractal noise. For instance, we confirmed a previous finding that multiplicative cascades show stronger t_{MF} signatures of nonlinearity with progressively more generations [80]. However, multifractal cascades generate much stronger t_{MF} signatures of nonlinearity with multifractal noise than with less multifractal IAAFT noise. This point extends the previous finding that multiplicative cascades involving fGn showed greater t_{MF} than multiplicative cascades with $awGn$ [80]. Hence, we may be able to rank-order the strength of multifractal nonlinearity from the greatest to the least for multiplicative cascades involving multifractal noise with wider spectra or more nonlinear temporal correlations towards multifractal noise with narrower spectra more closely approximating monofractal fGn as well as $awGn$. This work also informs this approach by indicating that noise with greater multifractal spectrum width (e.g., in the comparison between nonlinearly multifractal noise and IAAWT noise) and greater nonlinear temporal correlations (i.e., in the contrast between nonlinearly multifractal noise and IAAFT noise) can promote specifically different forms of ergodicity breaking.

This more nuanced cascade modeling respects that organisms are not monoliths but richly textured and task-sensitive ensembles of many degrees of freedom [111,112]. We mean

"degrees of freedom" not in the statistical sense (e.g., "$N - 1$") but in the thermodynamics and movement-science connotation of all those details of the system that can vary and are available for a controller or context to release constraints. Organisms thrive on their fluid capacity to gather and release their degrees of freedom with constraints they can build or break according to task demands [113–116], that is, organisms marshal their degrees of freedom through interactions across scales, exemplifying cascade form [117]. The observable interacts with various degrees of freedom, receiving stimulation such as innervations, collisions, and suggestions. These interactions, coupled with the task context, lead to the emergence of new adaptive behaviors that subsequently influence the entire system [118–125].

Network science has already begun to invoke multifractality as an elegant operationalization of the cascade relationships that might coordinate an organism's distribution of degrees of freedom—a point that appears theoretically [110] and empirically [46–64]. Also, multifractality may entail more about the broader system than a single observable can embody. We know that the extended systems behind our observables can have a spatiotemporal structure more globally [126], and we know that fractal structure has even supported the theoretical expectation that we should be able to unpack more global dynamics from the lower-dimensional projection of these dynamics appearing in our single observables [127]. Presumably, we have not been lucky enough to pick only the observables with multifractal structure; presumably, the multifractal structure is a more generic property of the whole organismic system. The hierarchical structure implicit in any observable is unlikely to belong strictly to that observable but sooner reflects the aggregates wielding that observable. Hence, we reserve a hope that the multifractal structure of any single observable should bear traces of the activity of other observables throughout the system. We expect that the multifractal structure of any single observable could thus carry, at the same time, echoes of the broader system that contains it and echoes of the novel contacts that it engages in. For instance, we collected full-body motion data from human participants during a perceptual task [61,128]. Basic network analyses examining the full array of bodywide markers revealed pervasive connections among anatomical components, showing widespread effects of current multifractality in one observable on subsequent multifractality in another. The empirical evidence suggests that multifractality at any single observable may bear the imprint of multifractality elsewhere.

A longer range goal is to establish principled expectations for a network of multifractal observables. How should multifractality spread? What potentially cascading spatiotemporal constraints might govern that spreading? In one sense, the insights available from studying a single observable's multifractality have potentially blossomed beyond the earlier possibilities that, say, more or less multifractality is associated with health (e.g., Refs. [129–131]). Yes, the nonlinear properties of a single observable may carry traces of a whole body's functioning [71,72,132–135]. But with these concerns in mind, global coherence of organism-wide coordination may be intermittent with the loosening of constraints according to task needs. Nonetheless, multifractal models might support predictions about the long-range patterns of such intermittency (e.g., single degrees of freedom in a complex movement system) in which we can begin to model how a single multifractal observable is a participating member of an ensemble. One observable might stand alone in a theoretical vacuum, but it might also be a particle modeled as part of a loosely interactive ensemble. Loose interactions among observables within the ensemble allow that. For instance, simulation work investigating single cascade processes has been crucial for understanding the sequential variations of a single human's forefinger pressing a button, for example, to signal their estimation of 1-s intervals [136,137]. This strategy is central to furthering a cascade-dynamical portrayal of the finger behavior in that task. However, in this example, the pressing of a fingertip is only the most immediate point of contact between the whole organism and the task environment. As we acknowledge that the single button press is only the tip of an organism-wide iceberg, we recognize that the pressing of the fingertip emerges lawfully from a vast network of anticipatory postural adaptations and longer-range postures distributed across the whole movement system [118–125]. Presumably, what we see in the single observable is the endogenous flow of coordinating cascades from neighboring or connected observables endogenous to the organism and any exogenous stimulation (e.g., Refs. [70,73–75]). The foregoing evidence from multifractal estimates from the brain and body could indicate cascades spreading from one observable to the next. That spatiotemporal spreading of cascades through the organism could provide a way to explain these anticipatory adaptations at many spatial and temporal scales. But again, the major challenge that future work needs to overcome is that we have no theoretical guide to our expectations of diagnosing these organism-wide flows from individual-observable multifractal results.

Hence, the present simulation work is a critical step in establishing an interactive framework to understand the adaptive functions of organisms, for instance, perceiving, acting, and cognizing. Instead of presenting a novel concept, we have clarified how we might interpret multifractal results when expecting our cascadelike measurements to bear the multifractal imprints of cascade processes elsewhere within the same body. The next steps for this process involve elaborating beyond the strictly additive and strictly multiplicative (e.g., Ref. [83]) and also developing the structure of multifractal noise to simulate different network relationships feeding into the cascade simulation (see also Refs. [70,73–75]). We hope also to explore the possibility that multifractally nonlinear signatures of cascade dynamics might help to classify qualitatively different modes of biological motility [45]. Behind this prospect is the further goal to connect our work with the network modeling that already provides glimmers of the relationship between distributed coordination and multifractal cascades [110]. A longer-range goal of this work would be to develop and empirically test predictions of how well multifractal nonlinearity can detect changes in cascade structure due to endogenous multifractal behavior of the organismal network, especially as it may change with network topology or with successful goal satisfaction. At that point, it might even be possible to begin sketching out methods for simulating exogenous perturbations that could begin to

develop theoretical predictions for how external threats or pressures might reshape the cascades that organismal networks of observables wield (cf. Refs. [70,73–75]). Such theoretical advances would welcome support for the growing empirical attempt to elaborate so-called "stochastic resonance" or "noise-based" stimulation beyond the classically "white-noise" *awGn* structure [138–146] to more endogenously naturalistic fractal and multifractal types of stimulation [70,73–75,147,148]. To summarize, the simulations herein furnish a sturdy theoretical foundation that aligns with current interpretations of multifractal nonlinearity and can root further work to articulate the cascade dynamics spanning diverse spatial and temporal scales within biological and psychological processes.

ACKNOWLEDGMENTS

This work was supported by the Center of Research in Human Movement Variability at the University of Nebraska at Omaha, funded by the National Institute of General Medical Sciences (NIGMS; Grant No. P20GM109090).

The authors have no conflict of interest.

[1] E. Jablonkaa, Interacting networks in social landscapes: A devo-evo approach to socialcultural dynamics, Hum. Dev. **67**, 288 (2023).

[2] D. J. Nicholson and J. Dupré, *Everything Flows: Towards a Processual Philosophy of Biology* (Oxford University Press, New York, 2018).

[3] B. J. West, The fractal tapestry of life: II Entailment of fractional oncology by physiology networks, Front. Netw. Physiol. **2**, 845495 (2022).

[4] A. G. Cherstvy, A. V. Chechkin, and R. Metzler, Anomalous diffusion and ergodicity breaking in heterogeneous diffusion processes, New J. Phys. **15**, 083039 (2013).

[5] A. G. Cherstvy and R. Metzler, Nonergodicity, fluctuations, and criticality in heterogeneous diffusion processes, Phys. Rev. E **90**, 012134 (2014).

[6] E. L. Hamaker, C. V. Dolan, and P. C. Molenaar, Statistical modeling of the individual: Rationale and application of multivariate stationary time series analysis, Multivar. Behav. Res. **40**, 207 (2005).

[7] J.-H. Jeon, V. Tejedor, S. Burov, E. Barkai, C. Selhuber-Unkel, K. Berg-Sørensen, L. Oddershede, and R. Metzler, *In vivo* anomalous diffusion and weak ergodicity breaking of lipid granules, Phys. Rev. Lett. **106**, 048103 (2011).

[8] J. L. Lebowitz and O. Penrose, Modern ergodic theory, Phys. Today **26**(2), 23 (1973).

[9] J. Li, J. Xie, A. Godec, K. R. Weninger, C. Liu, J. C. Smith, and L. Hong, Non-ergodicity of a globular protein extending beyond its functional timescale, Chem. Sci. **13**, 9668 (2022).

[10] R. Metzler, J.-H. Jeon, A. G. Cherstvy, and E. Barkai, Anomalous diffusion models and their properties: Non-stationarity, non-ergodicity, and ageing at the centenary of single particle tracking, Phys. Chem. Chem. Phys. **16**, 24128 (2014).

[11] P. C. M. Molenaar, A manifesto on psychology as idiographic science: Bringing the person back into scientific psychology, this time forever, Measurement **2**, 201 (2004).

[12] P. C. Molenaar, On the implications of the classical ergodic theorems: Analysis of developmental processes has to focus on intra-individual variation, Dev. Psychobiol. **50**, 60 (2008).

[13] P. Molenaar, K. O. Sinclair, M. J. Rovine, N. Ram, and S. E. Corneal, Analyzing developmental processes on an individual level using nonstationary time series modeling, Dev. Psychobiol. **45**, 260 (2009).

[14] P. C. Molenaar and C. G. Campbell, The new person-specific paradigm in psychology, Curr. Direct. Psychol. Sci. **18**, 112 (2009).

[15] C. T. Kello, G. G. Anderson, J. G. Holden, and G. C. Van Orden, The pervasiveness of 1/f scaling in speech reflects the metastable basis of cognition, Cognit. Sci. **32**, 1217 (2008).

[16] J. G. Holden, G. C. Van Orden, and M. T. Turvey, Dispersion of response times reveals cognitive dynamics, Psychol. Rev. **116**, 318 (2009).

[17] S. Lovejoy and D. Schertzer, Generalized scale invariance in the atmosphere and fractal models of rain, Water Resour. Res. **21**, 1233 (1985).

[18] S. Lovejoy and D. Schertzer, *The Weather and Climate: Emergent Laws and Multifractal Cascades* (Cambridge University Press, Cambridge, MA, 2018).

[19] E. Waymire, Scaling limits and self-similarity in precipitation fields, Water Resour. Res. **21**, 1271 (1985).

[20] K. Cuevas and A. Sheya, Ontogenesis of learning and memory: Biopsychosocial and dynamical systems perspectives, Dev. Psychobiol. **61**, 402 (2019).

[21] J. Fodor and M. Piattelli-Palmarini, *What Darwin Got Wrong* (Profile Books, London, 2011).

[22] G. Gottlieb, Probabilistic epigenesis, Dev. Sci. **10**, 1 (2007).

[23] K. N. Laland, T. Uller, M. W. Feldman, K. Sterelny, G. B. Müller, A. Moczek, E. Jablonka, and J. Odling-Smee, The extended evolutionary synthesis: Its structure, assumptions and predictions, Proc. R. Soc. B **282**, 20151019 (2015).

[24] R. C. Lewontin, Organism and environment, in *Learning, Development, and Culture*, edited by H. C. Plotkin (Wiley, Chichester, UK, 1982), pp. 151–170.

[25] S. Oyama, *Evolution's Eye: A Systems View of the Biology-Culture Divide* (Duke University Press, Durham, NC, 2000).

[26] S. Oyama, R. D. Gray, and P. E. Griffiths, *Cycles of Contingency: Developmental Systems and Evolution* (MIT Press, Cambridge, MA, 2003).

[27] E. Thelen and L. B. Smith, *A Dynamic Systems Approach to the Development of Cognition and Action* (MIT Press, Cambridge, MA, 1994).

[28] M. T. Turvey and A. Sheya, Non-obvious influences on perception-action abilities, Psychon. Bull. Rev. **24**, 1597 (2017).

[29] J. B. Wagman and D. B. Miller, Nested reciprocities: The organism–environment system in perception–action and development, Dev. Psychobiol. **42**, 317 (2003).

[30] J. A. Glazier, S. Raghavachari, C. L. Berthelsen, and M. H. Skolnick, Reconstructing phylogeny from the multifractal spectrum of mitochondrial DNA, Phys. Rev. E **51**, 2665 (1995).

[31] R. E. Plotnick and J. J. Sepkoski, A multiplicative multifractal model for originations and extinctions, Paleobiology **27**, 126 (2001).

[32] G. C. Van Orden, J. G. Holden, and M. T. Turvey, Self-organization of cognitive performance, J. Exp. Psychol. **132**, 331 (2003).

[33] C. Xue, Z. Liu, and N. Goldenfeld, Scale-invariant topology and bursty branching of evolutionary trees emerge from niche construction, Proc. Natl. Acad. Sci. USA **117**, 7879 (2020).

[34] M. J. Denton, P. K. Dearden, and S. J. Sowerby, Physical law *not natural selection* as the major determinant of biological complexity in the subcellular realm: New support for the pre-Darwinian conception of evolution by natural law, Biosystems **71**, 297 (2003).

[35] J. S. Kelso, K. Holt, P. Kugler, and M. Turvey, 2 On the concept of coordinative structures as dissipative structures: II. Empirical lines of convergence, in *Advances in Psychology*, Vol. 1 (Elsevier, Amsterdam, 1980), pp. 49–70.

[36] P. N. Kugler, J. S. Kelso, and M. T. Turvey, 1 On the concept of coordinative structures as dissipative structures: I. Theoretical lines of convergence, in *Advances in Psychology*, Vol. 1 (Elsevier, Amsterdam, 1980), pp. 3–47.

[37] P. N. Kugler, J. S. Kelso, and M. T. Turvey, On the control and coordination of naturally developing systems, Dev. Movement Contr. Coord. **5**, 1 (1982).

[38] B. B. Mandelbrot, Intermittent turbulence in self-similar cascades: Divergence of high moments and dimension of the carrier, J. Fluid Mech. **62**, 331 (1974).

[39] D. Sornette, *Critical Phenomena in Natural Sciences: Chaos, Fractals, Selforganization and Disorder: Concepts and Tools* (Springer Science & Business Media, New York, NY, 2006).

[40] A. Chhabra and R. V. Jensen, Direct determination of the f (α) singularity spectrum, Phys. Rev. Lett. **62**, 1327 (1989).

[41] D. G. Kelty-Stephen and M. Mangalam, Fractal and multifractal descriptors restore ergodicity broken by non-Gaussianity in time series, Chaos, Solitons Fract. **163**, 112568 (2022).

[42] D. G. Kelty-Stephen and M. Mangalam, Multifractal descriptors ergodically characterize non-ergodic multiplicative cascade processes, Physica A **617**, 128651 (2023).

[43] M. Mangalam and D. G. Kelty-Stephen, Point estimates, Simpson's paradox, and nonergodicity in biological sciences, Neurosci. Biobehav. Rev. **125**, 98 (2021).

[44] M. Mangalam and D. G. Kelty-Stephen, Ergodic descriptors of non-ergodic stochastic processes, J. R. Soc., Interface **19**, 20220095 (2022).

[45] M. Mangalam, R. Metzler, and D. G. Kelty-Stephen, Ergodic characterization of nonergodic anomalous diffusion processes, Phys. Rev. Res. **5**, 023144 (2023).

[46] M. P. Furmanek, M. Mangalam, D. G. Kelty-Stephen, and G. Juras, Postural constraints recruit shorter-timescale processes into the non-Gaussian cascade processes, Neurosci. Lett. **741**, 135508 (2021).

[47] D. G. Kelty-Stephen, M. P. Furmanek, and M. Mangalam, Multifractality distinguishes reactive from proactive cascades in postural control, Chaos Solitons Fract. **142**, 110471 (2021).

[48] M. Mangalam and D. G. Kelty-Stephen, Hypothetical control of postural sway, J. R. Soc., Interface **18**, 20200951 (2021).

[49] M. Mangalam, I.-C. Lee, K. M. Newell, and D. G. Kelty-Stephen, Visual effort moderates postural cascade dynamics, Neurosci. Lett. **742**, 135511 (2021).

[50] O. Kardan, K. C. Adam, I. Mance, N. W. Churchill, E. K. Vogel, and M. G. Berman, Distinguishing cognitive effort and working memory load using scale-invariance and alpha suppression in EEG, NeuroImage **211**, 116622 (2020).

[51] O. Kardan, A. J. Stier, E. A. Layden, K. W. Choe, M. Lyu, X. Zhang, S. L. Beilock, M. D. Rosenberg, and M. G. Berman, Improvements in task performance after practice are associated with scale-free dynamics of brain activity, Netw. Neurosci. **7**, 1129 (2023).

[52] J. R. Anastas, D. G. Kelty-Stephen, and J. A. Dixon, Executive function as an interaction-dominant process, Ecol. Psychol. **26**, 262 (2014).

[53] J. A. Dixon, J. G. Holden, D. Mirman, and D. G. Stephen, Multifractal dynamics in the emergence of cognitive structure, Top. Cogn. Sci. **4**, 51 (2012).

[54] D. G. Stephen, J. R. Anastas, and J. A. Dixon, Scaling in cognitive performance reflects multiplicative multifractal cascade dynamics, Front. Physiol. **3**, 102 (2012).

[55] C. A. Bell, N. S. Carver, J. A. Zbaracki, and D. G. Kelty-Stephen, Non-linear amplification of variability through interaction across scales supports greater accuracy in manual aiming: Evidence from a multifractal analysis with comparisons to linear surrogates in the Fitts task, Front. Physiol. **10**, 998 (2019).

[56] L. Bloomfield, E. Lane, M. Mangalam, and D. G. Kelty-Stephen, Perceiving and remembering speech depend on multifractal nonlinearity in movements producing and exploring speech, J. R. Soc., Interface **18**, 20210272 (2021).

[57] N. S. Carver, D. Bojovic, and D. G. Kelty-Stephen, Multifractal foundations of visually-guided aiming and adaptation to prismatic perturbation, Hum. Mov. Sci. **55**, 61 (2017).

[58] N. Jacobson, Q. Berleman-Paul, M. Mangalam, D. G. Kelty-Stephen, and C. Ralston, Multifractality in postural sway supports quiet eye training in aiming tasks: A study of golf putting, Hum. Mov. Sci. **76**, 102752 (2021).

[59] D. G. Kelty-Stephen, I. C. Lee, N. S. Carver, K. M. Newell, and M. Mangalam, Multifractal roots of suprapostural dexterity, Hum. Mov. Sci. **76**, 102771 (2021).

[60] D. G. Kelty-Stephen and J. A. Dixon, Interwoven fluctuations during intermodal perception: Fractality in head sway supports the use of visual feedback in haptic perceptual judgments by manual wielding., J. Exp. Psychol. Hum. Percept. Perform. **40**, 2289 (2014).

[61] M. Mangalam, N. S. Carver, and D. G. Kelty-Stephen, Global broadcasting of local fractal fluctuations in a bodywide distributed system supports perception via effortful touch, Chaos Solitons Fract. **135**, 109740 (2020).

[62] M. Mangalam, N. S. Carver, and D. G. Kelty-Stephen, Multifractal signatures of perceptual processing on anatomical sleeves of the human body, J. R. Soc. Interface **17**, 20200328 (2020).

[63] M. Mangalam and D. G. Kelty-Stephen, Multiplicative-cascade dynamics supports whole-body coordination for perception via effortful touch, Hum. Mov. Sci. **70**, 102595 (2020).

[64] Z. Palatinus, D. G. Kelty-Stephen, J. Kinsella-Shaw, C. Carello, and M. T. Turvey, Haptic perceptual intent in quiet standing affects multifractal scaling of postural fluctuations, J. Exp. Psychol. Hum. Percept. Perform. **40**, 1808 (2014).

[65] D. G. Kelty-Stephen and M. Mangalam, Turing's cascade instability supports the coordination of the mind, brain, and behavior, Neurosci. Biobehav. Rev. **141**, 104810 (2022).

[66] D. G. Kelty-Stephen, Threading a multifractal social psychology through within-organism coordination to within-group interactions: A tale of coordination in three acts, Chaos Solitons Fract. **104**, 363 (2017).

[67] M. Turvey and C. Carello, Obtaining information by dynamic (effortful) touching, Phil. Trans. R. Soc. B **366**, 3123 (2011).

[68] J. B. Wagman, D. M. McBride, and A. J. Trefzger, Perceptual experience and posttest improvements in perceptual accuracy and consistency, Percept. Psychophys. **70**, 1060 (2008).

[69] D. G. Stephen, R. Arzamarski, and C. F. Michaels, The role of fractality in perceptual learning: Exploration in dynamic touch, J. Exp. Psychol. Hum. Percept. Perform. **36**, 1161 (2010).

[70] D. Kelty-Stephen, O. D. Similton, E. Rabinowitz, and M. Allen, Multifractal auditory stimulation promotes the effect of multifractal torso sway on spatial perception: Evidence from distance perception by blindwalking, Ecol. Psychol. **35**, 136 (2023).

[71] M. Mangalam, D. G. Kelty-Stephen, K. Kiyono, and N. Stergiou, Spatial variability and directional shifts in postural control in Parkinson's disease, Clin. Park. Relat. Disord. **10**, 100249 (2024).

[72] M. Mangalam, D. G. Kelty-Stephen, I. Seleznov, A. Popov, A. D. Likens, K. Kiyono, and N. Stergiou, Older adults and individuals with Parkinson's disease control posture along suborthogonal directions that deviate from the traditional anteroposterior and mediolateral directions, Sci. Rep. **14**, 4117 (2024).

[73] M. Mangalam, D. G. Kelty-Stephen, J. H. Sommerfeld, N. Stergiou, and A. D. Likens, Temporal organization of stride-to-stride variations contradicts predictive models for sensorimotor control of footfalls during walking, PLoS ONE **18**, e0290324 (2023).

[74] D. G. Stephen and J. A. Dixon, Strong anticipation: Multifractal cascade dynamics modulate scaling in synchronization behaviors, Chaos Solitons Fract. **44**, 160 (2011).

[75] R. M. Ward and D. G. Kelty-Stephen, Bringing the nonlinearity of the movement system to gestural theories of language use: Multifractal structure of spoken English supports the compensation for coarticulation in human speech perception, Front. Physiol. **9**, 1152 (2018).

[76] C. J. Keylock, Multifractal surrogate-data generation algorithm that preserves pointwise Hölder regularity structure, with initial applications to turbulence, Phys. Rev. E **95**, 032123 (2017).

[77] C. J. Keylock, Hypothesis testing for nonlinear phenomena in the geosciences using synthetic, surrogate data, Earth Space Sci. **6**, 41 (2019).

[78] E. A. F. E. Ihlen, Introduction to multifractal detrended fluctuation analysis in Matlab, Front. Physiol. **3**, 141 (2012).

[79] T. Schreiber and A. Schmitz, Improved surrogate data for nonlinearity tests, Phys. Rev. Lett. **77**, 635 (1996).

[80] M. Mangalam, A. D. Likens, and D. G. Kelty-Stephen, Multifractal nonlinearity as arobust estimator of multiplicative cascade dynamics, arXiv:2312.05653 (2023).

[81] V. Venema, S. Bachner, H. W. Rust, and C. Simmer, Statistical characteristics of surrogate data based on geophysical measurements, Nonlin. Process. Geophys. **13**, 449 (2006).

[82] V. Venema, S. Meyer, S. G. Garcìa, A. Kniffka, C. Simmer, S. Crewell, U. Löhnert, T. Trautmann, and A. Macke, Surrogate cloud fields generated with the iterative amplitude adapted Fourier transform algorithm, Tellus A: Dynam. Meteorol. Oceanogr. **58**, 104 (2006).

[83] D. G. Kelty-Stephen and M. Mangalam, Additivity suppresses multifractal nonlinearity due to multiplicative cascade dynamics, Physica A **637**, 129573 (2024).

[84] K. Kiyono, Z. R. Struzik, and Y. Yamamoto, Estimator of a non-Gaussian parameter in multiplicative log-normal models, Phys. Rev. E **76**, 041113 (2007).

[85] A. N. Kolmogorov, A refinement of previous hypotheses concerning the local structure of turbulence in a viscous incompressible fluid at high Reynolds number, J. Fluid Mech. **13**, 82 (1962).

[86] A. Obukhov, Some specific features of atmospheric turbulence, J. Geophys. Res. **67**, 3011 (1962).

[87] B. Castaing, Y. Gagne, and E. Hopfinger, Velocity probability density functions of high Reynolds number turbulence, Physica D **46**, 177 (1990).

[88] D. Schertzer and S. Lovejoy, Physical modeling and analysis of rain and clouds by anisotropic scaling multiplicative processes, J. Geophys. Res.: Atmos. **92**, 9693 (1987).

[89] S. M. Rytov, Y. A. Kravtsov, and V. I. Tatarskii, *Principles of Statistical Radiophysics: Wave Propagation Through Random Media*, Vol. 4 (Springer, Berlin, 1989).

[90] D. Thirumalai, R. D. Mountain, and T. R. Kirkpatrick, Ergodic behavior in supercooled liquids and in glasses, Phys. Rev. A **39**, 3563 (1989).

[91] B. B. Mandelbrot, *The Fractal Geometry of Nature*, Vol. 1 (W. H. Freeman, New York, 1982).

[92] T. C. Halsey, M. H. Jensen, L. P. Kadanoff, I. Procaccia, and B. I. Shraiman, Fractal measures and their singularities: The characterization of strange sets, Phys. Rev. A **33**, 1141 (1986).

[93] B. B. Mandelbrot, *Fractals and Scaling in Finance: Discontinuity, Concentration, Risk* (Springer, New York, 2013).

[94] M. Zamir, Critique of the test of multifractality as applied to biological data, J. Theor. Biol. **225**, 407 (2003).

[95] J.-F. Muzy, E. Bacry, and A. Arneodo, Multifractal formalism for fractal signals: The structure-function approach versus the wavelet-transform modulus-maxima method, Phys. Rev. E **47**, 875 (1993).

[96] N. Scafetta and P. Grigolini, Scaling detection in time series: Diffusion entropy analysis, Phys. Rev. E **66**, 036130 (2002).

[97] A. Bashan, R. Bartsch, J. W. Kantelhardt, and S. Havlin, Comparison of detrending methods for fluctuation analysis, Physica A **387**, 5080 (2008).

[98] K. E. Bassler, G. H. Gunaratne, and J. L. McCauley, Empirically based modeling in financial economics and beyond, and spurious stylized facts, Int. Rev. Financ. Anal. **17**, 767 (2008).

[99] M. Ignaccolo, M. Latka, and B. West, Detrended fluctuation analysis of scaling crossover effects, Europhys. Lett. **90**, 10009 (2010).

[100] A. Turiel, H. Yahia, and C. J. Pérez-Vicente, Microcanonical multifractal formalism—A geometrical approach to multifractal systems: Part i. Singularity analysis, J. Phys. A: Math. Theor. **41**, 015501 (2008).

[101] D. Schertzer and S. Lovejoy, Nonlinear geodynamical variability: Multiple singularities, universality and observables, in *Non-linear Variability in Geophysics: Scaling and Fractals*, edited by D. Schertzer and S. Lovejoy (Springer, Dordrecht, 1991), pp. 41–82.

[102] Y. He, S. Burov, R. Metzler, and E. Barkai, Random time-scale invariant diffusion and transport coefficients, Phys. Rev. Lett. **101**, 058101 (2008).

[103] W. Deng and E. Barkai, Ergodic properties of fractional Brownian-Langevin motion, Phys. Rev. E **79**, 011112 (2009).

[104] C. J. Morales and E. D. Kolaczyk, Wavelet-based multifractal analysis of human balance, Ann. Biomed. Eng. **30**, 588 (2002).

[105] D. Bates, M. Mächler, B. Bolker, and S. Walker, Fitting linear mixed-effects models using lme4, J. Stat. Softw. **67**, 1 (2015).

[106] R Core Team, R: A language and environment for statistical computing, R Version 4.0.4 (2024), https://www.R-project.org/.

[107] K. Kiyono, J. Hayano, E. Watanabe, Z. R. Struzik, and Y. Yamamoto, Non-Gaussian heart rate as an independent predictor of mortality in patients with chronic heart failure, Heart Rhythm **5**, 261 (2008).

[108] C. J. Keylock, Gradual multifractal reconstruction of time-series: Formulation of the method and an application to the coupling between stock market indices and their Hölder exponents, Physica D **368**, 1 (2018).

[109] K. Hu, P. C. Ivanov, Z. Chen, P. Carpena, and H. E. Stanley, Effect of trends on detrended fluctuation analysis, Phys. Rev. E **64**, 011114 (2001).

[110] X. Xiao, H. Chen, and P. Bogdan, Deciphering the generating rules and functionalities of complex networks, Sci. Rep. **11**, 22964 (2021).

[111] N. Bernstein, *The Co-ordination and Regulation of Movements* (Pergamon Press, Oxford, UK, 1996).

[112] N. A. Bernstein, *Dexterity and Its Development* (Lawrence Erlbaum, Mahwah, NJ, 1996).

[113] H. H. Pattee, The physics of symbols: Bridging the epistemic cut, Biosystems **60**, 5 (2001).

[114] H. H. Pattee, Laws, constraints, and the modeling relation–history and interpretations, Chem. Biodivers. **4**, 2272 (2007).

[115] H. H. Pattee, The physical basis and origin of hierarchical control, in *Laws, Language and Life: Howard Pattee's Classic Papers on the Physics of Symbols with Contemporary Commentary*, edited by H. H. Pattee and J. Rączaszek-Leonardi (Springer, Dordrecht, 2012), pp. 91–110.

[116] H. H. Pattee, Epistemic, evolutionary, and physical conditions for biological information, Biosemiotics **6**, 9 (2013).

[117] V. L. Profeta and M. T. Turvey, Bernstein's levels of movement construction: A contemporary perspective, Hum. Mov. Sci. **57**, 111 (2018).

[118] M. L. Latash, The Bernstein problem: How does the central nervous system make its choices, in *Dexterity and Its Development* (Psychology Press, New York, 1996), pp. 277–303.

[119] M. L. Latash, *Synergy* (Oxford University Press, New York, 2008).

[120] M. L. Latash, The bliss (not the problem) of motor abundance (not redundancy), Exp. Brain Res. **217**, 1 (2012).

[121] M. L. Latash, On primitives in motor control, Motor Contr. **24**, 318 (2020).

[122] M. L. Latash, What do synergies do at Bernstein's level of synergies?, in *Bernstein's Construction of Movements* (Routledge, New York, 2020), pp. 344–352.

[123] M. L. Latash and V. L. Talis, Bernstein's philosophy of time: An unknown manuscript by Nikolai Bernstein (1949), Motor Contr. **25**, 315 (2021).

[124] M. L. Latash, One more time about motor (and non-motor) synergies, Exp. Brain Res. **239**, 2951 (2021).

[125] S. Reschechtko and M. L. Latash, Stability of hand force production. II. Ascending and descending synergies, J. Neurophysiol. **120**, 1045 (2018).

[126] A. L. Goldberger, D. R. Rigney, and B. J. West, Chaos and fractals in human physiology, Sci. Am. **262**, 42 (1990).

[127] T. Sauer, J. A. Yorke, and M. Casdagli, Embedology, J. Stat. Phys. **65**, 579 (1991).

[128] M. Mangalam, R. Chen, T. R. McHugh, T. Singh, and D. G. Kelty-Stephen, Bodywide fluctuations support manual exploration: Fractal fluctuations in posture predict perception of heaviness and length via effortful touch by the hand, Hum. Mov. Sci. **69**, 102543 (2020).

[129] P. C. Ivanov, L. A. N. Amaral, A. L. Goldberger, S. Havlin, M. G. Rosenblum, Z. R. Struzik, and H. E. Stanley, Multifractality in human heartbeat dynamics, Nature (Lond.) **399**, 461 (1999).

[130] M. Mangalam, A. Sadri, J. Hayano, E. Watanabe, K. Kiyono, and D. G. Kelty-Stephen, Multifractal foundations of biomarker discovery for heart disease and stroke, Sci. Rep. **13**, 18316 (2023).

[131] H. Stanley, L. N. Amaral, A. Goldberger, S. Havlin, P. C. Ivanov, and C.-K. Peng, Statistical physics and physiology: Monofractal and multifractal approaches, Physica A **270**, 309 (1999).

[132] M. Mangalam, I. Seleznov, A. Popov, E. Kolosova, D. G. Kelty-Stephen, and K. Kiyono, Postural control in gymnasts: Anisotropic fractal scaling reveals proprioceptive reintegration in vestibular perturbation, Front. Physiol. **4**, 1393171 (2024).

[133] W. Rahman, S. Lee, M. S. Islam, V. N. Antony, H. Ratnu, M. R. Ali, A. A. Mamun, E. Wagner, S. Jensen-Roberts, E. Waddell *et al.*, Detecting parkinson disease using a web-based speech task: Observational study, J. Med. Internet Res. **23**, e26305 (2021).

[134] K. Sechidis, R. Fusaroli, J. R. Orozco-Arroyave, D. Wolf, and Y.-P. Zhang, A machine learning perspective on the emotional content of Parkinsonian speech, Artif. Intell. Med. **115**, 102061 (2021).

[135] A. Tsanas, M. A. Little, and L. O. Ramig, Remote assessment of Parkinson's disease symptom severity using the simulated cellular mobile telephone network, IEEE Access **9**, 11024 (2021).

[136] N. A. Kuznetsov and S. Wallot, Effects of accuracy feedback on fractal characteristics of time estimation, Front. Integr. Neurosci. **5**, 62 (2011).

[137] E. A. Ihlen and B. Vereijken, Multifractal formalisms of human behavior, Hum. Mov. Sci. **32**, 633 (2013).

[138] J. J. Collins, T. T. Imhoff, and P. Grigg, Noise-enhanced tactile sensation, Nature (Lond.) **383**, 770 (1996).

[139] J. J. Collins, T. T. Imhoff, and P. Grigg, Noise-enhanced information transmission in rat SA1 cutaneous mechanoreceptors via aperiodic stochastic resonance, J. Neurophysiol. **76**, 642 (1996).

[140] J. J. Collins, T. T. Imhoff, and P. Grigg, Noise-mediated enhancements and decrements in human tactile sensation, Phys. Rev. E **56**, 923 (1997).

[141] A. M. Galica, H. G. Kang, A. A. Priplata, S. E. D'Andrea, O. V. Starobinets, F. A. Sorond, L. A. Cupples, and L. A. Lipsitz, Subsensory vibrations to the feet reduce gait variability in elderly fallers, Gait Posture **30**, 383 (2009).

[142] M. D. McDonnell and D. Abbott, What is stochastic resonance? Definitions, misconceptions, debates, and its relevance to biology, PLoS Comput. Biol. **5**, e1000348 (2009).

[143] M. D. McDonnell and L. M. Ward, The benefits of noise in neural systems: Bridging theory and experiment, Nat. Rev. Neurosci. **12**, 415 (2011).

[144] D. L. Miranda, W.-H. Hsu, D. C. Gravelle, K. Petersen, R. Ryzman, J. Niemi, and N. Lesniewski-Laas, Sensory enhancing insoles improve athletic performance during a hexagonal agility task, J. Biomech. **49**, 1058 (2016).

[145] A. Priplata, J. Niemi, M. Salen, J. Harry, L. A. Lipsitz, and J. J. Collins, Noise-enhanced human balance control, Phys. Rev. Lett. **89**, 238101 (2002).

[146] A. A. Priplata, J. B. Niemi, J. D. Harry, L. A. Lipsitz, and J. J. Collins, Vibrating insoles and balance control in elderly people, Lancet **362**, 1123 (2003).

[147] M. J. Hove, K. Suzuki, H. Uchitomi, S. Orimo, and Y. Miyake, Interactive rhythmic auditory stimulation reinstates natural $1/f$ timing in gait of Parkinson's patients, PLoS ONE **7**, e32600 (2012).

[148] D. Nozaki, J. J. Collins, and Y. Yamamoto, Mechanism of stochastic resonance enhancement in neuronal models driven by $1/f$ noise, Phys. Rev. E **60**, 4637 (1999).

Correction: The captions to Figures 9 and 10 contained a typographical error and have been fixed.